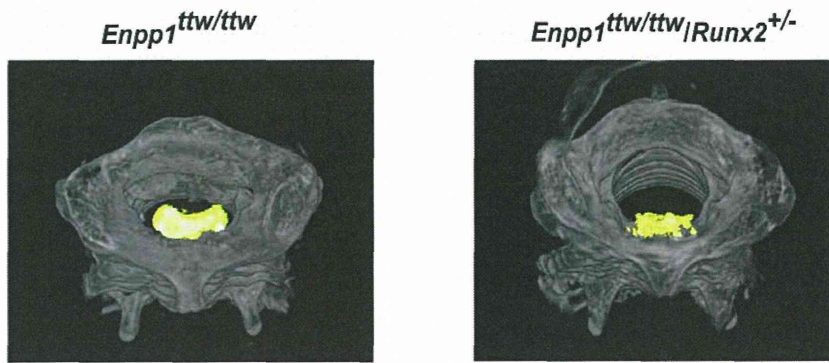
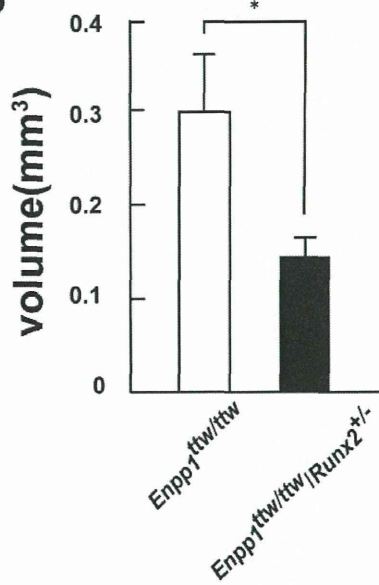


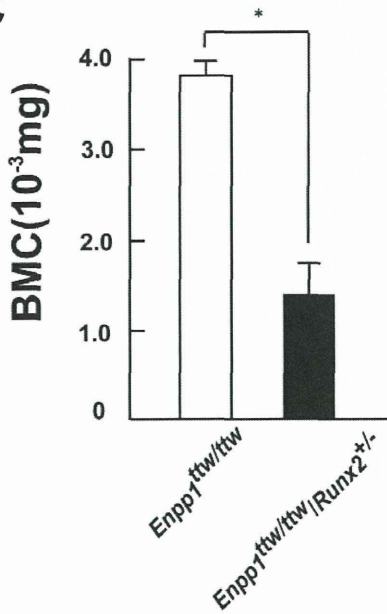
**A**



**B**



**C**



**D**

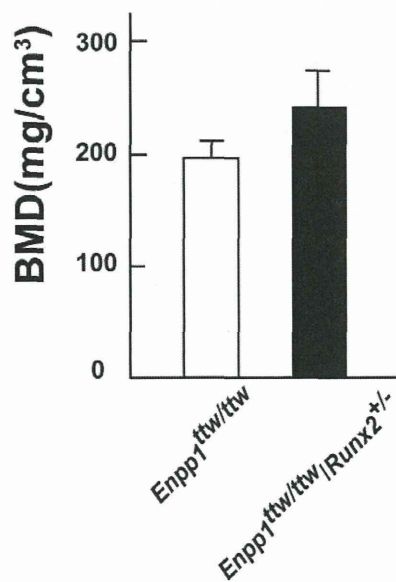


**Figure 3. Quantitative analysis of ossification by micro-computed tomography (CT).** A, Micro-computed tomography of the cervical spine of *Enpp1<sup>ttw/ttw</sup>* mice at 12 weeks of age with or without Runx2 haploinsufficiency. 3D reconstructed images. Ectopically calcified region is shown in yellow. B, Quantitative analysis of the ossification of the cruciform ligament at the atlanto-occipital area using micro-CT in *Enpp1<sup>ttw/ttw</sup>* mice at 8 weeks of age with or without Runx2 haploinsufficiency. Note a significant decrease in calcified region in *ENPP1<sup>ttw/ttw</sup>/Runx2<sup>+/-</sup>* mice. C, D Micro-CT analysis of the ossification of the cruciform ligament at the atlanto-occipital area in *Enpp1<sup>ttw/ttw</sup>* mice at 12 weeks of age with or without Runx2 haploinsufficiency. Bone mineral content (C) Bone mineral density (D). doi:10.1371/journal.pone.0043372.g003

fact, several studies have reported a decrease in MSX2 expression [20] or an increase in BMP2 expression [21] in the affected areas of OPLL patients.

To date, no specific treatment for OPLL has been developed. Inhibiting ectopic calcification by substances modulating mineralization such as pyrophosphate is expected to affect systemic bone mineralization [22]. In this paper, we showed that removing one allele of *Runx2* does not affect the degree of mineralization per unit volume, but only affects the arearize of ectopic bone formation. Thus, it is plausible that decreasing ectopic bone formation by inhibition of Runx2 expression may provide novel therapeutic

approaches for treating OPLL without affecting mineralization in surrounding normal bone.

### Acknowledgments

We thank to S. Sunamura and C. Ma for technical assistance.

### Author Contributions

Conceived and designed the experiments: MI YA KS AO ST. Performed the experiments: MI JP AK SS HO. Analyzed the data: MI HI. Wrote the paper: MI ST.

### References

- Inamasu J, Guiot BH, Sachs DC (2006) Ossification of the posterior longitudinal ligament: an update on its biology, epidemiology, and natural history. *Neurosurgery* 58: 1027–1039; discussion 1027–1039.
- Sakou T, Matsunaga S, Koga H (2000) Recent progress in the study of pathogenesis of ossification of the posterior longitudinal ligament. *J Orthop Sci* 5: 310–315.
- Ren Y, Feng J, Liu ZZ, Wan H, Li JH, et al. (2011) A new haplotype in BMP4 implicated in ossification of the posterior longitudinal ligament (OPLL) in a Chinese population. *J Orthop Res*.
- Kim DH, Jeong YS, Chon J, Yoo SD, Kim HS, et al. (2011) Association between interleukin 15 receptor, alpha (IL15RA) polymorphism and Korean patients with ossification of the posterior longitudinal ligament. *Cytokine* 55: 343–346.
- Kong Q, Ma X, Li F, Guo Z, Qi Q, et al. (2007) COL6A1 polymorphisms associated with ossification of the ligamentum flavum and ossification of the posterior longitudinal ligament. *Spine (Phila Pa 1976)* 32: 2834–2838.
- Kamiya M, Harada A, Mizuno M, Iwata H, Yamada Y (2001) Association between a polymorphism of the transforming growth factor-beta1 gene and genetic susceptibility to ossification of the posterior longitudinal ligament in Japanese patients. *Spine (Phila Pa 1976)* 26: 1264–1266; discussion 1266–1267.
- Horikoshi T, Maeda K, Kawaguchi Y, Chiba K, Mori K, et al. (2006) A large-scale genetic association study of ossification of the posterior longitudinal ligament of the spine. *Hum Genet* 119: 611–616.
- Yasui N, Ono K, Yamaura I, Konomi H, Nagai Y (1983) Immunohistochemical localization of types I, II, and III collagens in the ossified posterior longitudinal ligament of the human cervical spine. *Calcif Tissue Int* 35: 159–163.
- Komori T (2011) Signaling networks in RUNX2-dependent bone development. *J Cell Biochem* 112: 750–755.
- Otto F, Thornell AP, Crompton T, Denzel A, Gilmour KC, et al. (1997) *Cbfa1*, a candidate gene for cleidocranial dysplasia, is essential for osteoblast differentiation and bone development. *Cell* 89: 765–771.
- Okawa A, Nakamura I, Goto S, Moriya H, Nakamura Y, et al. (1998) Mutation in *Npps* in a mouse model of ossification of the posterior longitudinal ligament of the spine. *Nat Genet* 19: 271–273.
- Takeda S, Bonnamy JP, Owen MJ, Ducey P, Karsenty G (2001) Continuous expression of *Cbfa1* in nonhypertrophic chondrocytes uncovers its ability to induce hypertrophic chondrocyte differentiation and partially rescues *Cbfa1*-deficient mice. *Genes Dev* 15: 467–481.
- Kimura A, Inose H, Yano F, Fujita K, Ikeda T, et al. (2010) Runx1 and Runx2 cooperate during sternal morphogenesis. *Development* 137: 1159–1167.
- Sato S, Kimura A, Ozdemir J, Asou Y, Miyazaki M, et al. (2008) The distinct role of the Runx proteins in chondrocyte differentiation and intervertebral disc degeneration: Findings in murine models and in human disease. *Arthritis Rheum* 58: 2764–2775.
- Tanno M, Furukawa KI, Ueyama K, Harata S, Motomura S (2003) Uniaxial cyclic stretch induces osteogenic differentiation and synthesis of bone morphogenetic proteins of spinal ligament cells derived from patients with ossification of the posterior longitudinal ligaments. *Bone* 33: 475–484.
- Liu Y, Zhao Y, Chen Y, Shi G, Yuan W (2010) RUNX2 polymorphisms associated with OPLL and OLF in the Han population. *Clin Orthop Relat Res* 468: 3333–3341.
- Kishiyama M, Sawada T, Kanemaru K, Kudo H, Numasawa T, et al. (2008) A functional RNAi screen for Runx2-regulated genes associated with ectopic bone formation in human spinal ligaments. *J Pharmacol Sci* 106: 404–414.
- Iwasaki K, Furukawa KI, Tanno M, Kusumi T, Ueyama K, et al. (2004) Uniaxial cyclic stretch induces *Cbfa1* expression in spinal ligament cells derived from patients with ossification of the posterior longitudinal ligament. *Calcif Tissue Int* 74: 448–457.
- Ikeda R, Yoshida K, Tsukahara S, Sakamoto Y, Tanaka H, et al. (2005) The promyelotic leukemia zinc finger promotes osteoblastic differentiation of human mesenchymal stem cells as an upstream regulator of *CBFA1*. *J Biol Chem* 280: 8523–8530.
- Yoshizawa T, Takizawa F, Iizawa F, Ishibashi O, Kawashima H, et al. (2004) Homeobox protein MSX2 acts as a molecular defense mechanism for preventing ossification in ligament fibroblasts. *Mol Cell Biol* 24: 3460–3472.
- Tanaka H, Nagai E, Murata H, Tsubone T, Shirakura Y, et al. (2001) Involvement of bone morphogenetic protein-2 (BMP-2) in the pathological ossification process of the spinal ligament. *Rheumatology (Oxford)* 40: 1163–1168.
- Addison WN, Azari F, Sorensen ES, Kaartinen MT, McKee MD (2007) Pyrophosphate inhibits mineralization of osteoblast cultures by binding to mineral, up-regulating osteopontin, and inhibiting alkaline phosphatase activity. *J Biol Chem* 282: 15872–15883.

[ Case Report ]

**Incidental discovery of an intradural extramedullary tumor  
during imaging studies of a traumatic injury at the  
same spinal level: a case report**

**Takeo Furuya, Yoshikazu Tsuneizumi, Osamu Ikeda, Akihiko Okawa<sup>1)</sup>**

**Shunichi Kunishi, Jo Katsuragi, Mitsutoshi Ohta, Kazuhisa Takahashi<sup>1)</sup>**

**Masashi Yamazaki<sup>1)</sup> and Toshio Ohi**

Department of Orthopaedic Surgery, Kamitsuga General Hospital, Tochigi 322-8550.

<sup>1)</sup>Department of Orthopedic Surgery, Graduate School of Medicine, Chiba University, Chiba 260-8670.

(Received August 21, 2012, Accepted August 30, 2012)

**SUMMARY**

A 72-year-old man with a history of fall was admitted to our institute. Neurological testing demonstrated motor weakness of left upper limbs, showing grade 3/5 muscle strength for wrist and fingers. He had no sensory loss in his trunk or bilateral upper and lower extremities. Deep tendon reflexes were normal in both upper and lower extremities. Babinski signs were positive bilaterally. Radiologic examination showed fractures of cervical spine at the C3 and C6 levels which we classified as stage 3 compressive flexion fractures under the Allen classification system. Magnetic resonance imaging (MRI) showed a space-occupying lesion in the vertebral canal at the C3/4 level. We initially diagnosed the mass as a traumatic spinal subdural or subarachnoid hematoma. Diachronic MRI evaluation and enhanced-MRI and CT myelogram established the diagnosis of an intradural extramedullary tumor. To the best of our knowledge, no report has previously described finding an intradural extramedullary tumor incidentally during imaging studies of a traumatic injury at the same spinal level. Our experience suggests that the presence of atypical findings, such as oval shape, in a posttraumatic space-occupying spinal lesion should lead clinicians to consider the possibility that the lesion may be a tumor rather than a hematoma.

**Key words:** intradural extramedullary tumor, schwannoma, neurilemmoma, trauma, diagnosis, spinal hematoma

---

*Address correspondence to* Dr. Takeo Furuya.

Department of Orthopedic Surgery, Graduate School of Medicine, Chiba University, 1-8-1 Inohana, Chuo-ku, Chiba 260-8670, Japan.

Phone: +81-43-226-2117. Fax: +81-43-226-2116.

E-mail: takeo1225@snow.plala.or.jp

## I. Introduction

Intradural extramedullary tumors are generally slow growing and usually diagnosed only after they begin to cause symptoms such as local pain or neurological disturbances. However, such spinal cord tumors are sometimes discovered incidentally in association with trauma, screening magnetic resonance imaging (MRI). We now report a case of an intradural extramedullary tumor discovered incidentally during imaging studies of a traumatic injury at the same spinal level.

## II. Case Report

A 72-year-old man with a history of fall from stairs was admitted with incomplete left hemiplegia. He had a past medical history of intracerebral hemorrhage. He had no history of anticoagulant therapy. Routine blood tests, including coagulative parameters, were normal. Neurological testing demonstrated motor weakness of left upper limbs, showing grade 3/5 muscle strength, and left lower extremities showing grade 4/5 muscle strength. He had no sensory loss in his trunk or bilateral upper and lower extremities. Deep tendon reflexes were normal in both upper and lower extremities. Babinski signs were positive bilaterally. Radiologic examination detected swelling of the retropharyngeal space, along with a fracture line (called 'fracture of the beak') running from the anterior of the C3 vertebral body to the C3/4 intervertebral disk, plus a C4 spinous process fracture (Fig. 1). A sagittal computed tomography (CT) image revealed the same type of fracture at C6 as seen at C3, along with spinous process fractures at C4, C7, Th1, and Th2 (Fig. 1). We thus classified these fractures as stage 3 compressive flexion fractures under the Allen classification system. Midsagittal and axial MRI views showed a space-occupying lesion in the vertebral canal located on the middle to left side at the C3/4 level that showed isointensity with the spinal cord on T1-weighted images and high intensity on T2-weighted images (Fig. 2). The mass had an oval shape and appeared to be located in the subdural or subarachnoid space. At a glance the mass looked 'classic' for an intradural tumor,

we made an initial clinical diagnosis of either traumatic spinal subdural hematoma (SDH) or subarachnoid hematoma (SAH) because of the present history and the location of the mass. Because our patient had relatively minimal neurological symptoms, we initially chose a conservative approach in which we treated him by a

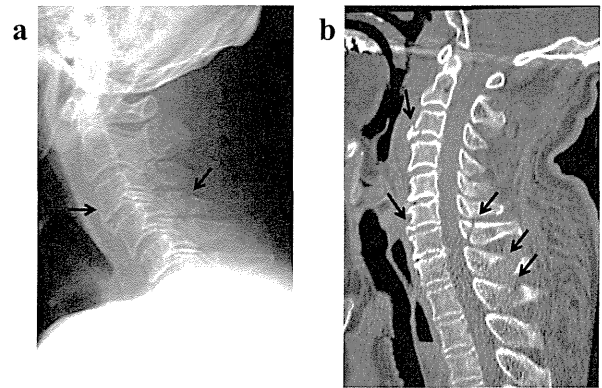


Fig. 1 (a) X-p and (b) computed tomographic images of the cervical spine following spinal trauma in a 72-year-old man show injury to the C3 & C6 vertebral bodies which we classified as stage 3 compressive flexion fractures under the Allen classification system. Arrows denote the vertebral body and spinous process fractures.

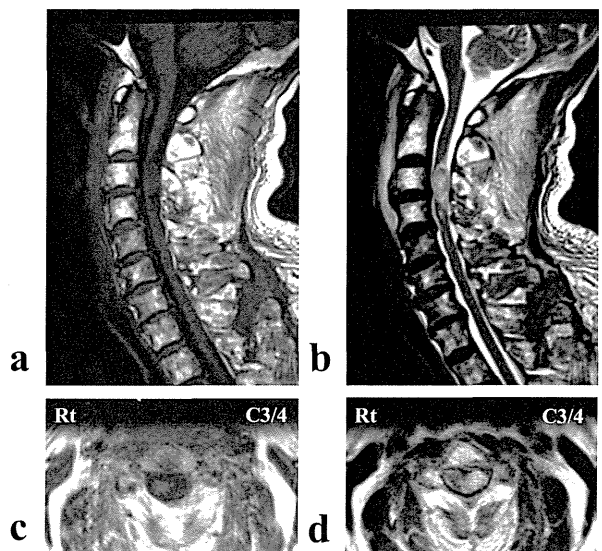


Fig. 2 (a) T1-weighted midsagittal and (b) T2-weighted midsagittal of magnetic resonance imaging at the time of admission demonstrated a space-occupying lesion in the vertebral canal at the C3/4 level that showed an isointensity with the spinal cord on T1-weighted images and a high intensity on T2-weighted images. (c) T1-weighted axial and (d) T2-weighted axial views showed a round mass located on the left side of the spinal cord.

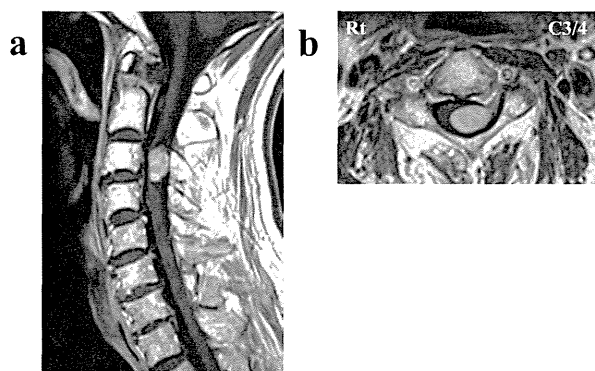


Fig. 3 (a) T1-weighted midsagittal and (b) axial views of magnetic resonance imaging at the C3/4 level after injection of Gd-DTPA show definite enhancement of the mass.

halo-vest and Philadelphia collar with the expectation that the mass would spontaneously regress over time. However, MRI one week after the injury and one month after the injury still showed no reduction in size and no signal change. MRI one month after the injury showed enhancement of the mass after intravenous administration of gadopentetate dimeglumine (Gd-DTPA) (Fig. 3). A CT myelogram at this time revealed the presence of an intradural extramedullary tumor.

Having diagnosed this mass as an intradural extramedullary tumor, we proceeded to surgery because the tumor was causing extensive spinal cord compression. We performed a left hemilaminectomy of C2-6 with excising the tumor en-bloc under microscopy. The pathological diagnosis was schwannoma. No postsurgical neurological deficits resulted from the tumor excision. MRI after surgery showed no tumor recurrence and adequate decompression of the spinal cord. Follow-up examination six months after the surgery found that the patient had returned to his pre-injury activities of daily living level.

### III. Discussion

Reviewing the imaging studies for our patient, we can identify several findings that helped with refuting the assumption that the mass lesion was a hematoma at an earlier period. First, the oval shape of the mass in the initial MR images was atypical for traumatic hematoma, as spinal SDH and spinal SAH usually spread

longitudinally. Furthermore, the ongoing minimal degree of observed neurological impairment was discordant with the high level of spinal cord compression by the mass seen on MRI. That is, if the cord compression had occurred rapidly, as from a hematoma, more serious neurological symptoms should have soon developed in response. These two findings, then, should at least raise a suspicion that the mass was something other than a hematoma.

However, the strongest evidence against the mass being a hematoma developed over time, as subsequent MRI studies continued to show no change in the size or intensity of the mass. Prior reports observed that traumatic hematomas do spontaneously resolve [1,2]. The lack of intensity change is particularly important in ruling out hematoma, as hemoglobin degrades to deoxyhemoglobin, methemoglobin, and hemosiderin over time, and each of these compounds have differing MRI absorption spectra. Thus the failure to observe intensity changes would imply that the mass was not a hematoma.

Spinal cord tumors are sometimes discovered after trauma [3-5]. In this case, we definitively ruled out hematoma by performing enhanced-MRI. Although we possibly might have diagnosed the tumor a bit earlier had we initially considered the possibility of a tumor and performed enhanced-MRI sooner, the clinical history of trauma implicated hematoma as the most likely cause at the outset. The diagnosis of tumor resulted largely from ongoing observation of neurological symptoms and repeated MRI evaluations over time.

To the best of our knowledge, this is the first report that describes the incidental discovery of an intradural extramedullary tumor during imaging studies of a traumatic injury at the same spinal level. In this case, we arrived at the correct diagnosis through diachronic MRI evaluation and enhanced-MRI, following which we successfully excised the tumor. Our experience with this patient leads us to conclude that enhanced-MRI can be a useful tool for diagnosing spinal tumors even in trauma cases. Furthermore, the differential diagnosis of space-occupying posttraumatic spinal lesions should include at least the possibility of a tumor as well as hematoma.

**References**

- 1) Russell NA, Mangan MA. Acute spinal cord compression by subarachnoid and subdural hematoma occurring in association with brachial plexus avulsion. Case report. *J Neurosurg* 1980; 52: 410-3.
  - 2) Russell NA, Benoit BG. Spinal subdural hematoma; a review. *Surg Neurol* 1983; 20: 133-7.
  - 3) Honda E, Fujisawa H, Koyama T, Oshima Y, Sugita Y, Abe T. Symptomatic spinal arachnoid cyst triggered by seat belt injury-case report. *Neurol Med Chir (Tokyo)* 1998; 38: 168-72.
  - 4) Fedakar R, Akan O, Eren B. Cervical schwannoma presenting with trauma-induced neurological symptoms. *Acta Orthop Traumatol Turc* 2008; 42: 208-10.
  - 5) Sharifi G, Mortaz M, Parsaei B. Multiple intradural extramedullary tumours presenting with paraplegia after trauma. *Acta Neurochir (Wien)* 2009; 151: 697-8.
-

# Granulocyte Colony-Stimulating Factor (G-CSF) Protects Oligodendrocyte and Promotes Hindlimb Functional Recovery after Spinal Cord Injury in Rats

Ryo Kadota<sup>1</sup>, Masao Koda<sup>2\*</sup>, Junko Kawabe<sup>1</sup>, Masayuki Hashimoto<sup>3</sup>, Yutaka Nishio<sup>1</sup>, Chikato Mannoji<sup>2</sup>, Tomohiro Miyashita<sup>1</sup>, Takeo Furuya<sup>1</sup>, Akihiko Okawa<sup>1</sup>, Kazuhisa Takahashi<sup>1</sup>, Masashi Yamazaki<sup>1</sup>

<sup>1</sup>Department of Orthopaedic Surgery, Chiba University Graduate School of Medicine, Chuo-Ku, Chiba, Japan, <sup>2</sup>Department of Orthopaedic Surgery, Chiba Aoba Municipal Hospital, Chuo-Ku, Chiba, Japan, <sup>3</sup>Department of Orthopaedic Surgery, Chiba Medical Center, Chuo-Ku, Chiba, Japan

## Abstract

**Background:** Granulocyte colony-stimulating factor (G-CSF) is a protein that stimulates differentiation, proliferation, and survival of cells in the granulocytic lineage. Recently, a neuroprotective effect of G-CSF was reported in a model of cerebral infarction and we previously reported the same effect in studies of murine spinal cord injury (SCI). The aim of the present study was to elucidate the potential therapeutic effect of G-CSF for SCI in rats.

**Methods:** Adult female Sprague-Dawley rats were used in the present study. Contusive SCI was introduced using the Infinite Horizon Impactor (magnitude: 200 kilodyne). Recombinant human G-CSF (15.0 µg/kg) was administered by tail vein injection at 1 h after surgery and daily the next four days. The vehicle control rats received equal volumes of normal saline at the same time points.

**Results:** Using a contusive SCI model to examine the neuroprotective potential of G-CSF, we found that G-CSF suppressed the expression of pro-inflammatory cytokine (IL-1 beta and TNF- alpha) in mRNA and protein levels. Histological assessment with luxol fast blue staining revealed that the area of white matter spared in the injured spinal cord was significantly larger in G-CSF-treated rats. Immunohistochemical analysis showed that G-CSF promoted up-regulation of anti-apoptotic protein Bcl-XL on oligodendrocytes and suppressed apoptosis of oligodendrocytes after SCI. Moreover, administration of G-CSF promoted better functional recovery of hind limbs.

**Conclusions:** G-CSF protects oligodendrocyte from SCI-induced cell death via the suppression of inflammatory cytokines and up-regulation of anti-apoptotic protein. As a result, G-CSF attenuates white matter loss and promotes hindlimb functional recovery.

**Citation:** Kadota R, Koda M, Kawabe J, Hashimoto M, Nishio Y, et al. (2012) Granulocyte Colony-Stimulating Factor (G-CSF) Protects Oligodendrocyte and Promotes Hindlimb Functional Recovery after Spinal Cord Injury in Rats. PLoS ONE 7(11): e50391. doi:10.1371/journal.pone.0050391

**Editor:** Valentin Ceña, Universidad de Castilla-La Mancha, Spain

**Received:** November 25, 2011; **Accepted:** October 24, 2012; **Published:** November 27, 2012

**Copyright:** © 2012 Kadota et al. This is an open-access article distributed under the terms of the Creative Commons Attribution License, which permits unrestricted use, distribution, and reproduction in any medium, provided the original author and source are credited.

**Funding:** This work was supported by grants-in-aid for Scientific Research from the Ministry of Education, Science and Culture of Japan (16591473-00) and 21st Century Development Grant of Cervical Spine Research Society 2006. The funders had no role in study design, data collection and analysis, decision to publish, or preparation of the manuscript.

**Competing Interests:** The authors have declared that no competing interests exist.

\* E-mail: masaokod@gmail.com

## Introduction

Acute spinal cord injury (SCI) is divided into two pathological phases termed primary and secondary injury [1]. The primary injury consists of focal tissue destruction caused by direct mechanical trauma. This physical insult then initiates the second phase of injury which is a pathophysiological reaction of spinal cord. Apoptosis of neurons and glial cells left intact by the initial trauma occurs during the secondary phase. In addition, oligodendrocytes distant from the immediate site of injury undergo apoptosis. Maximal cell death occurs one week after injury and leads directly to demyelination [2]. Several *in vivo* studies have demonstrated that the amount of spared white matter correlates to residual locomotor function [3,4]. Thus, protection of oligodendrocytes from apoptotic cell death might reduce demyelination and improve functional recovery. Many factors could exacerbate

the secondary phase of injury, including vascular changes, increased concentrations of free radicals and free fatty acids, ionic mechanisms of axonal injury, glutamate excitotoxicity, and immune and inflammatory reactions [5]. Currently, high-dose methylprednisolone (MP) in acute SCI is an accepted treatment for attenuation of secondary injury [6]. However, it has become controversial in recent years due to the risk of serious adverse effects and its modest neurological benefits [7]. Therefore, development of new drug therapies which can substitute for high-dose MP is an area of intense study.

Granulocyte colony-stimulating factor (G-CSF) is a 19.6 kDa glycoprotein that was initially identified as a serum factor that induced differentiation of a murine myelomonocytic leukemic cell line [8]. It is widely known as a hematopoietic cytokine that promotes survival, proliferation and differentiation of cells of the



neutrophil lineage [8,9]. It is used clinically for patients with leukocytopenia and for donors of peripheral blood-derived hematopoietic progenitor cells prior to collection for transplantation [10].

Within the central nervous system (CNS), G-CSF has pleiotropic actions. In recent years, the beneficial effects of G-CSF have been demonstrated in rodent stroke models [11–15]. Moreover, clinical trials of G-CSF for stroke reported its safety and feasibility [16]. In the case of SCI, several research groups including us previously reported that G-CSF treatment promoted functional recovery in the mouse and rat SCI models [17–22].

Although the beneficial effects of G-CSF on neurons are partially understood, little is known about G-CSF-mediated reduction of apoptosis of oligodendrocytes after SCI. Therefore we hypothesized that G-CSF could attenuate apoptosis of oligodendrocytes and, as a result, improve white matter preservation and functional recovery. This may represent another mechanism by which G-CSF provides neuroprotection following SCI. In the present study, our aim was to assess the anti-apoptotic effects of G-CSF on oligodendrocytes and to elucidate the mechanism using the rat contusive SCI model.

## Results

### G-CSF Receptor (G-CSFR) Expression

To assess the expression of G-CSFR, we performed immunofluorescence analysis on histological sections of spinal cords. The data revealed that G-CSFR was expressed on neurons, astrocytes and oligodendrocytes in normal spinal cord (Fig. S1A–C). One week after injury, G-CSFR was expressed on glial fibrillary acidic protein (GFAP)-positive astrocytes and myelin oligodendrocyte-specific protein (MOSP)-positive oligodendrocytes (Fig. 1). Quantification of G-CSFR/MOSP double-positive cells showed significant increase of the number of MOSP-positive oligodendrocytes in the G-CSF-treated group 2 mm rostral and caudal to the epicenter (Fig. S1D). Almost all of MOSP-positive oligodendrocytes expressed G-CSFR in both the vehicle and G-CSF groups (Fig. S1D).

### Expression of Inflammatory Cytokines after SCI

To detect the anti-inflammatory effects of G-CSF in the SCI model, we performed Real-Time PCR for interleukin 1-beta (IL-1 $\beta$ ), tumor necrosis factor-alpha (TNF- $\alpha$ ), FAS, FAS ligand (FASL), interferon-gamma (IFN- $\gamma$ ), matrix metalloproteinase-2 (MMP2) and matrix metalloproteinase-9 (MMP9) (Fig. 2). The study revealed that 12 h after surgery, expression of IL-1 $\beta$  and TNF- $\alpha$  mRNAs was significantly suppressed in the G-CSF group (Fig. 2 A, B, closed columns) compared to the vehicle control group (Fig. 2 A, B, open columns). Specifically, expression of IL-1 $\beta$  mRNA in the G-CSF group was 3.36-fold lower than in the vehicle group (Fig. 2 A,  $p < 0.05$ ). For TNF- $\alpha$  mRNA in the G-CSF group, expression was 1.98-fold lower than in the vehicle group (Fig. 2 B,  $p < 0.05$ ). Twenty-four h and 72 h following surgery, expression of IL-1 $\beta$  and TNF- $\alpha$  mRNAs tended to be lower than controls; however, the differences were not statistically significant. The results of Real-Time PCR for the other factors showed no significant difference between the vehicle and G-CSF-treated groups.

To further confirm G-CSF-mediated attenuation of SCI-induced up-regulation of IL-1 $\beta$  and TNF- $\alpha$ , we performed western blot analysis for IL-1 $\beta$  and TNF- $\alpha$  on protein samples extracted from spinal cord with or without G-CSF treatment 24 and 72 h following spinal cord injury. Western blot analysis

revealed that G-CSF suppressed protein expression of IL-1 $\beta$  and TNF- $\alpha$  72 hours after the injury (Fig. 2C, D,  $p < 0.05$ ).

### Enumeration of Early Inflammatory Leukocytes and Microglia/macrophages

Immunohistochemistry for IL-1 $\beta$  and myeloperoxidase (MPO, a marker for leukocyte) revealed that the frequencies of cells positive for MPO were not statistically different in the two groups 12 and 24 h after surgery (data not shown). In contrast, the frequencies of cells positive for both IL-1 $\beta$  and MPO was significantly smaller in the G-CSF group than in the vehicle group 12 and 24 h after surgery (Fig. 3D). Twelve hours after surgery, the mean numbers of double positive cells per section in the G-CSF group were  $52 \pm 3.8$  in 2 mm rostral to the epicenter and  $56 \pm 2.5$  in 2 mm caudal to the epicenter, respectively (Fig. 3D). In contrast, the frequencies of double positive cells in the vehicle group were considerably higher 12 hours after surgery ( $103 \pm 4.0$  per section in 2 mm rostral to the epicenter and  $118 \pm 5.3$  per section in 2 mm caudal to the epicenter, respectively; Fig. 3D). Twenty-four hours after the injury, the G-CSF group showed decrease of the number of IL-1 $\beta$  and MPO double-positive cells as same as 12 hours after injury (Fig. 3D). Double immunofluorescence study for ionized calcium-binding adaptor molecule 1 (Iba-1, as a marker for activated microglia and macrophages) and inducible nitric oxide synthase (iNOS, as a marker for Th1-driven activation of microglia/macrophages) or arginase-1 (a marker for Th2-driven activation of microglia/macrophages) was performed to elucidate G-CSF-mediated reaction and phenotypic alteration of macrophage/microglia. The number of Iba-1-positive cells in the G-CSF group was significantly smaller than that in the vehicle group in the rostral and caudal segments (Fig. S3), whereas the ratios between iNOS and arginase-1 did not change in both the vehicle and G-CSF groups in lesioned spinal cord at any segments observed (Fig. S3).

### Suppressed Apoptosis of Oligodendrocytes

Near the epicenter of the injury, apoptotic oligodendrocytes (adenomatous polyposis coli; APC<sup>+</sup> and caspase 3<sup>+</sup> cells) were observed (Fig. 4 A–C, arrowheads). The percentages of apoptotic oligodendrocytes were significantly smaller in the G-CSF group than that in the vehicle group both 72 h and 1 week after surgery. Specifically, 72 hours after surgery, the mean percentages of apoptotic oligodendrocytes among the sections were 32.0% in the G-CSF group and 47.8% in the vehicle group (Fig. 4 D). The percentages of apoptotic oligodendrocytes were significantly suppressed in most sections: 4 mm and 6 mm rostral to the epicenter ( $p < 0.05$ ) and 6 mm caudal to the epicenter ( $p < 0.01$ ). Significance was not reached for the section 4 mm caudal to the epicenter. One week after surgery, the mean percentages of apoptotic oligodendrocytes among sections were 13.9% in the G-CSF group and 35.2% in the vehicle group (Fig. 4 E). The percentages of apoptotic oligodendrocytes were significantly suppressed in all of the sections: 6 mm rostral to the epicenter ( $p < 0.05$ ), and 4 mm rostral and 4 mm and 6 mm caudal to the epicenter ( $p < 0.01$ ). To further confirm the results of immunohistochemistry for apoptotic oligodendrocytes, we performed double immunofluorescence study for MOSP as another marker for oligodendrocytes and activated caspase-3 as a marker for apoptotic cells (Fig. S4). The staining pattern was similar to that of the double fluorescence study for APC and activated caspase-3, suggesting that the data of apoptotic oligodendrocytes were convincing.

There was no APC- and Bcl-XI-double positive cells in vehicle control rats 1 week after injury (Fig. 4 I–K), whereas a part of



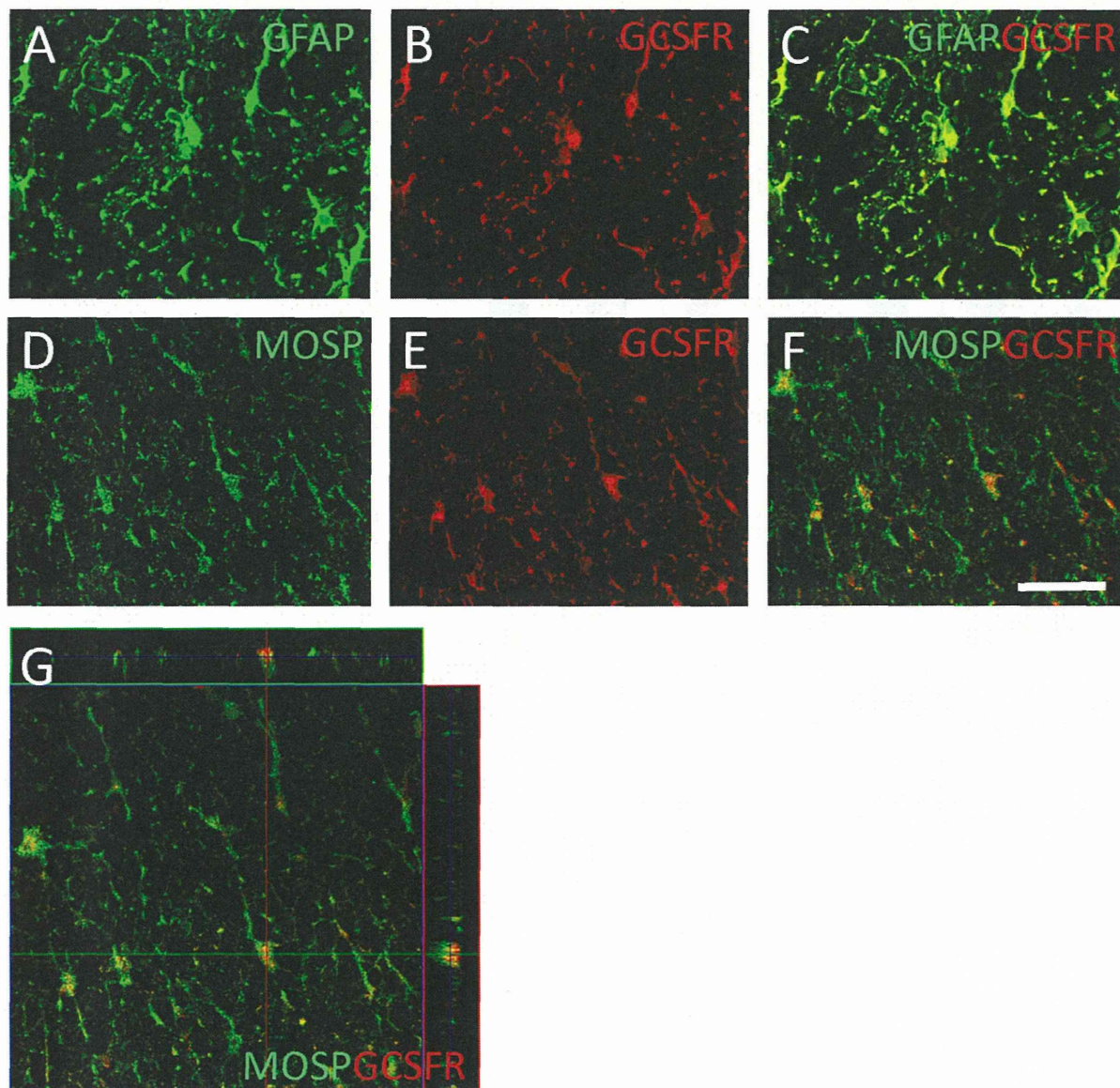


**Figure 1. Granulocyte colony-stimulating factor receptor (G-CSFR) expression.** Immunofluorescent double labeling for G-CSFR and cell-specific markers 1 week after surgery in vehicle-treated rats. Double-positive cells for G-CSFR and glial fibrillary acidic protein (GFAP, marker for astrocytes; A–C) and G-CSFR and myelin oligodendrocyte specific protein (MOSP, marker for oligodendrocytes; D–G) were detected. To show colocalization precisely, positive signal for G-CSFR/GFAP and G-CSFR/MOSP were detected using confocal laser microscopy (A–F) and 3-dimensional image was reconstructed (G). Bars = 50  $\mu$ m.  
doi:10.1371/journal.pone.0050391.g001

APC-positive cells simultaneously expressed Bcl-Xl in G-CSF-treated rat 1 week after injury (average 31.8% of APC-positive cells expressed Bcl-Xl, Fig. 4F–H).

The number of MAP-2-positive neurons was significantly larger in the G-CSF group than that in the vehicle group in the rostral and caudal segments to the lesion epicenter (Fig. S2).

#### White Matter Sparing after SCI

Luxol fast blue (LFB) staining 6 weeks after injury revealed better myelin integrity and preservation in G-CSF-administered rats in increased magnification of the section (Fig. 5C, D, 4 mm caudal to epicenter). The percentage of normal-appearing myelin in the G-CSF group (Fig. 5E, closed columns) was significantly

higher than that in the vehicle group (Fig. 5E, open columns) in all the segments analyzed except for the lesion epicenter.

Immunohistochemistry for myelin basic protein (MBP) 6 weeks after injury showed preservation of myelin sheath in G-CSF-treated animals. The number of MBP-positive myelin sheath in the G-CSF group (Fig. 5H, K and Fig. 5L, closed columns) was significantly larger than that in the vehicle group (Fig. 5G, J and Fig. 5L, open columns).

#### Recovery of Hindlimb Motor Function

All rats had a full score (21 points) prior to surgery, and the score dropped to zero immediately after SCI. Hindlimb function showed a significant recovery in rats in the G-CSF group six weeks after surgery compared with that of the vehicle group (Fig. 6A).

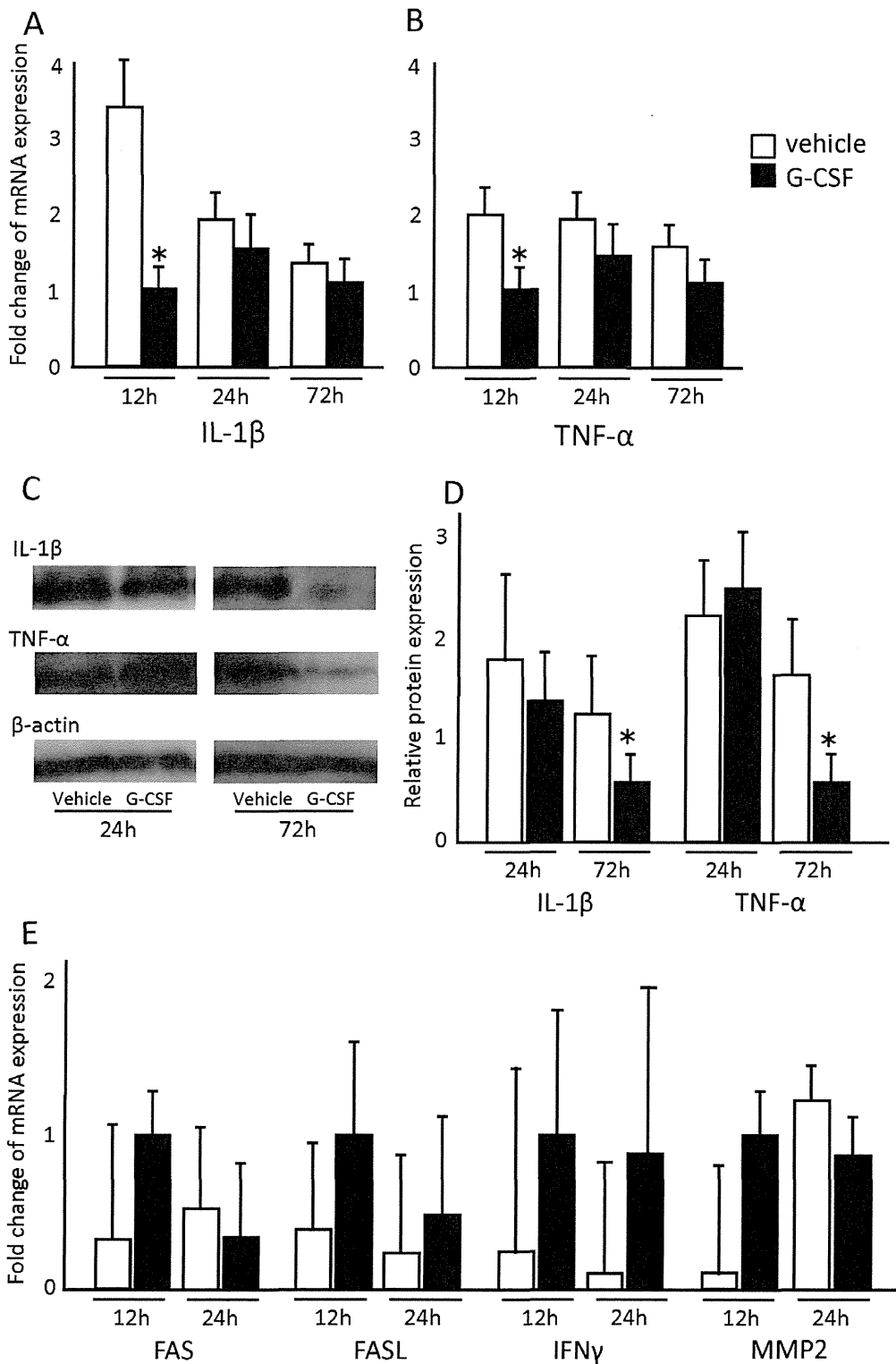


**Figure 2. G-CSF suppressed pro-inflammatory cytokine expression.** Real time quantitative PCR and western blot analysis were performed to quantify mRNA and protein expression of pro-inflammatory cytokines in the acute phase of spinal cord injury. Values obtained were normalized to value of 18S ribosomal RNA expression and were expressed as the fold-increase over values of the G-CSF group 12 hours after surgery. The expression of interleukin-1 beta (IL-1  $\beta$ , A) and tumor necrosis factor-alpha (TNF- $\alpha$ , B) mRNA was significantly suppressed in the G-CSF group (closed column) compared with the vehicle group (open column) 12 hours after surgery. Western blot analysis revealed that G-CSF suppressed the expression level of IL-1  $\beta$  (C, upper row right, D, closed column,  $p < 0.05$ ) and TNF- $\alpha$  (C, middle row right, D, closed column,  $p < 0.05$ ). There was no significant difference between the vehicle and G-CSF groups in mRNA expression of FAS, FASL, IFN- $\gamma$ , MMP-2 and MMP-9. Values are mean  $\pm$  SEM. \* $p < 0.05$ . doi:10.1371/journal.pone.0050391.g002



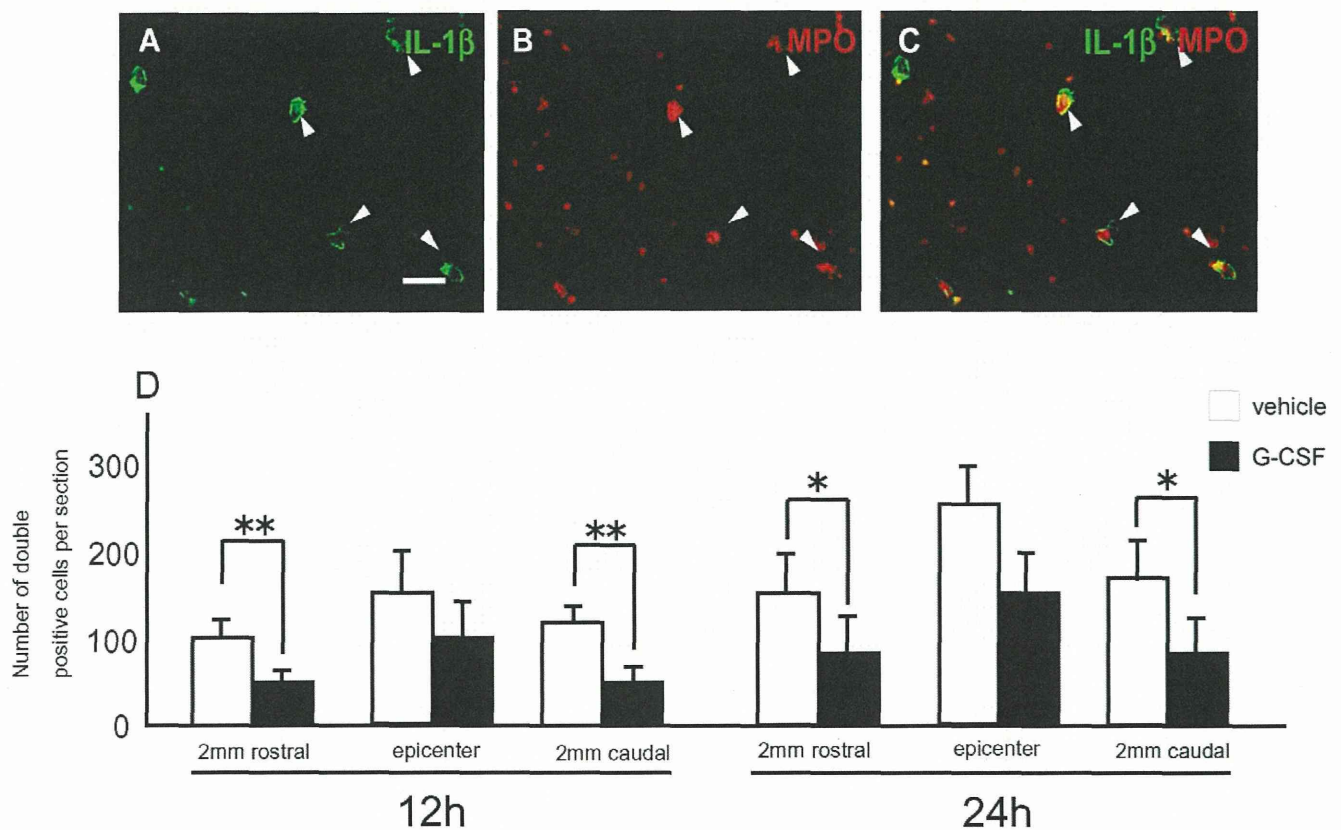


**Figure 3. G-CSF decreased the number of IL- $\beta$  expressing leukocytes.** Immunohistochemistry for IL- $\beta$  and myeloperoxidase (MPO) in the acute phase of injury. Near the lesion epicenter, IL- $\beta$ -positive round cells were also positive for MPO, a marker for leukocytes (A–C, arrowheads). The number of double positive cells for IL- $\beta$  and MPO was significantly smaller in the G-CSF group (D, closed column) than in the vehicle group (D, open column). Bars = 50  $\mu$ m. Values are mean  $\pm$  SEM. \* $p < 0.05$ . doi:10.1371/journal.pone.0050391.g003

The average recovery score six weeks post-surgery was significantly higher in the G-CSF group (Fig. 6B, closed circle,  $p < 0.01$ ) than the vehicle group (Fig. 6B, open circle). The average final score in the G-CSF group was  $12.5 \pm 0.9$  (9 to 16), indicating frequent (51–94%) to consistent weight-supported plantar steps and occasional (<50%) forelimb-hindlimb coordination. In contrast, the score was  $9.5 \pm 0.3$  (7 to 13) in the control group, indicating plantar placement of the paw with weight support in stance only (i.e., when stationary) or occasional, frequent, or consistent (95–100%) weight-supported dorsal stepping and no plantar stepping. The mean value of the inclined plane test was significantly higher in the G-CSF group than in the vehicle group (50.0 to 31.7, Fig. 6C,  $p < 0.01$ ). Finally, there was good correlation between the percentage of normal myelin and the final motor function score ( $r = 0.676$ ,  $p < 0.01$ , not shown). Those results showed that five days treatment with G-CSF had an impact on the animal status six weeks later.

## Discussion

The present results showed the beneficial effects of G-CSF in the setting of SCI. G-CSF significantly reduced injury-induced up-regulation of IL-1 $\beta$  and TNF- $\alpha$  expression in mRNA and protein levels and the number of infiltrating leukocytes and activated microglia/macrophages which potentially involve in SCI-induced inflammatory reactions. Furthermore, early treatment with G-CSF significantly attenuated subsequent apoptosis of oligodendrocytes

and white matter degeneration, and promoted better long-term functional recovery of the hindlimbs.

It is believed that the injury-induced up-regulation of inflammatory cytokines substantially contributes to secondary injury following SCI. Exogenous administration of IL-1 $\beta$  has been shown to exacerbate ischemic damage, whereas administration of an endogenous IL-1 $\beta$  receptor antagonist [23] or a neutralizing antibody [24] reduced brain damage and edema when administered before a stroke in rats. Previous reports showed that G-CSF mediates anti-inflammatory effects after a variety of infections [25]. G-CSF decreases monocytic production of pro-inflammatory cytokines such as IL-1 $\beta$  and TNF- $\alpha$  *in vitro* [25,26]. And, *in vivo* studies showed that G-CSF also suppresses the expression of IL-1 $\beta$  in a cerebral infarct model [11] and TNF- $\alpha$  in experimental encephalomyelitis [24]. In the current study, G-CSF significantly reduced the expression of IL-1 $\beta$  and TNF- $\alpha$  mRNA in the acute phase after SCI. Moreover, results of immunofluorescence double staining for IL-1 $\beta$  and MPO suggest that G-CSF reduced inflammatory cytokine expression by neutrophils, whereas G-CSF had no influence on the extent of neutrophil infiltration. The discrepancy between the results of real-time PCR and immunofluorescence may be caused by the time lag between transcription and translation. The results obtained here conflict with a report that G-CSF reduced neutrophil infiltration in a model of splanchnic ischemia and reperfusion [27]. This discrepancy might be caused by general differences between the experimental models and/or unique microenvironments within the organs. Furthermore, the present results showed that G-CSF decreased the

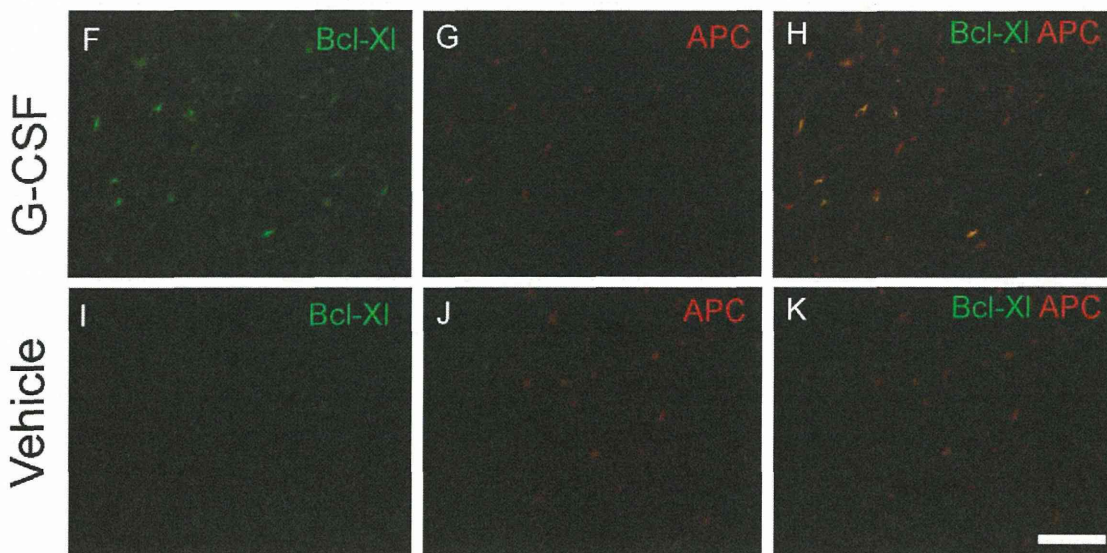
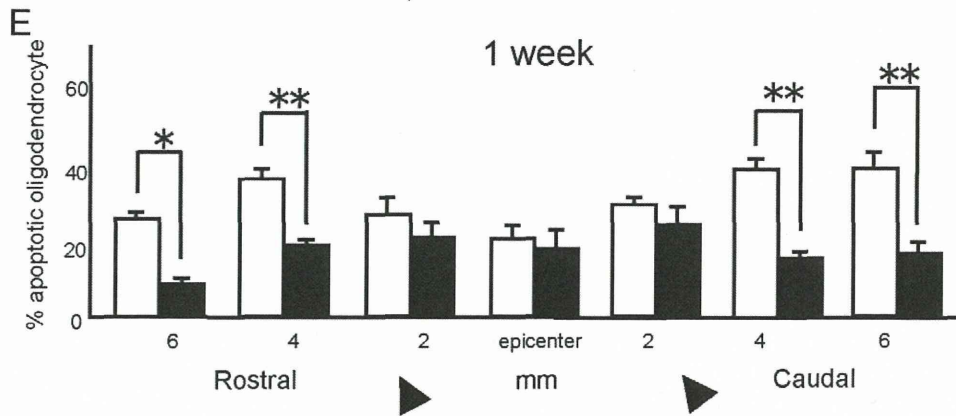
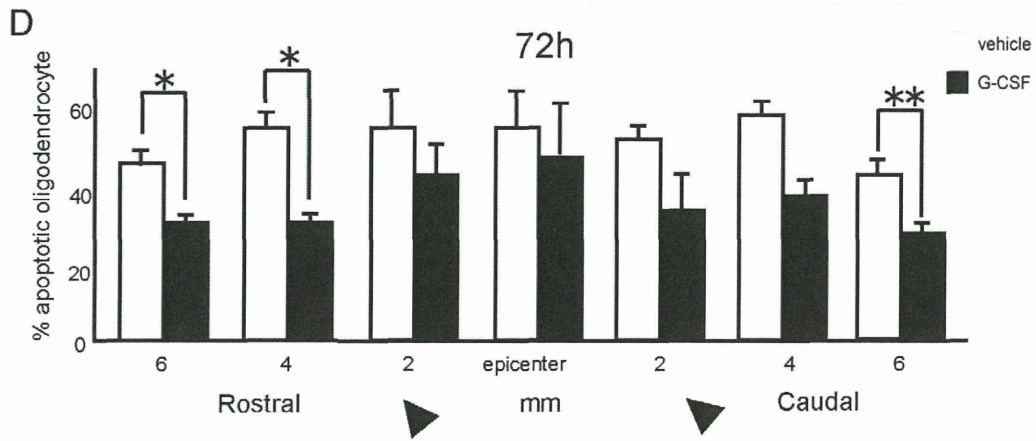
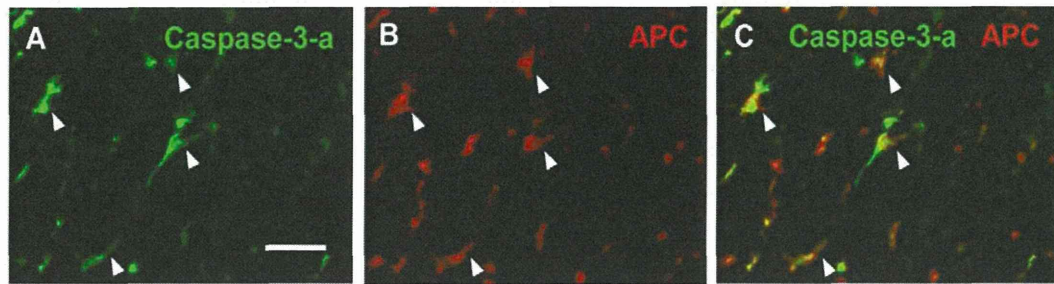


**Figure 4. G-CSF suppressed apoptosis of oligodendrocytes and promoted anti-apoptotic protein Bcl-XI on oligodendrocytes.** Immunohistochemistry for adenomatous polyposis coli (APC; a marker for oligodendrocytes) and activated caspase 3 (a marker for apoptotic cells) in the acute phase of spinal cord injury. Representative figure of cells double-positive for APC and activated caspase 3 in the vehicle group 4 mm rostral to the lesion epicenter 1 week after injury is shown (A–C, arrowheads). The percentage of apoptotic oligodendrocytes was significantly smaller in the G-CSF group (closed column) than that in the vehicle group (open column) 72 hours (D) and one week (E) after surgery. In vehicle-treated control rats, Bcl-XI/APC doubler-positive cells were not detected (I–K). In contrast, Bcl-XI/APC doubler-positive Bcl-XI expressing oligodendrocytes were observed in the spinal cord of G-CSF-treated rats (F–H). Bars = 50  $\mu$ m (A–C) and 100  $\mu$ m (F–K). Values are mean  $\pm$  SEM. \* $p$ <0.05, \*\* $p$ <0.01. doi:10.1371/journal.pone.0050391.g004

number of activated microglia/macrophages. Microglia/macrophages can involve inflammatory reaction in injured spinal cord. Therefore this data might suggest the other possible anti-inflammatory action of G-CSF.

G-CSF has direct neuroprotective effects against glutamate-induced neuronal death and stroke [11–15,28]. G-CSF elicits its anti-apoptotic effects on neurons via activation of proteins of the STAT family or the PI3-K/Akt pathway, similar to anti-apoptotic effects on neutrophils [13]. In this study of spinal cord injury in the rat, G-CSFR was expressed in neurons, astrocytes and oligodendrocytes, but not in microglia. SCI promoted up-regulation of G-CSFR expression in astrocytes and oligodendrocytes. Moreover, G-CSF treatment did not alter the expression pattern of G-CSFR. Thus, the reduction of oligodendrocyte apoptosis by G-CSF was possibly achieved by several mechanisms as followings. Firstly, G-CSF-mediated suppression of inflammatory cytokine expression might attenuate apoptosis of oligodendrocytes because these inflammatory cytokines are potentially toxic for oligodendrocytes [29,30]. Secondly, G-CSF-mediated up-regulation of anti-apoptotic proteins in oligodendrocytes might suppress apoptosis. The present results of immunofluorescence double labelling for APC and Bcl-XI revealed G-CSF-mediated up-regulation of Bcl-XI in oligodendrocytes. This data is in line with the G-CSF-mediated up-regulation of Bcl-XI gene expression in spinal cord partial transection model [21]. Finally, G-CSF-mediated attenuation of neuronal death, which action we previously reported [19], and/or promotion of neurite outgrowth [21] could enhance survival of oligodendrocytes because the survival of oligodendrocytes depends on stimuli from axons [31]. The present data of G-CSF-mediated attenuation of loss of MAP-2- positive neurons might support that hypothesis.

The present results showed that G-CSF suppresses apoptosis of oligodendrocytes and white matter degeneration after SCI. There was a direct correlation between the area of spared myelin and final motor function score. This result is in line with previous reports [32,33] and explains how G-CSF promotes functional recovery. In the murine SCI model, we previously reported that G-CSF attenuates apoptosis of neurons via the activation of signaling pathways downstream from the G-CSFR [19]. Taken together, G-CSF exerts neuroprotective effects for neurons and oligodendrocytes via anti-inflammatory and anti-apoptotic actions, resulting in reduced white matter degeneration and promotion of functional recovery. Other than the anti-inflammatory or anti-apoptotic effects on the CNS, G-CSF can promote mobilization of bone marrow-derived stem cells and their migration into injured spinal cord tissues and promote functional recovery [18,20]. Furthermore, G-CSF has several actions on the vascular system. For example, G-CSF suppresses brain edema formation after stroke [11] and promotes angiogenesis in stroke [28] and SCI [17] models. Finally, G-CSF stimulates neurogenesis both directly [13] or via the up-regulation of vascular endothelial growth factor [34]. All of those mechanisms could potentially contribute to the neuroprotective effects of G-CSF following SCI.

In terms of safety and efficacy, G-CSF has an excellent record in clinical use. In the case of stroke, STAIR presents criteria for drug development [35] and G-CSF fulfills those criteria well. Briefly,

those criteria include the following: i) blood-brain barrier penetration, ii) neuroprotective activity in different stroke models including permanent ischemia demonstrated by independent groups, iii) activity shown in different species, iv) well-known pharmacokinetics, and v) functional outcome data. In this context, G-CSF may be a candidate for clinical application in the setting of acute SCI. In that regard, the therapeutic time window is important. In the rat photothrombotic stroke model, G-CSF administered 72 h after induction of ischemia for ten days improved recovery [36]. G-CSF administration might be effective if delayed even further. Additional studies are needed to define the therapeutic time window of G-CSF treatment for SCI. G-CSF is an attractive candidate for treatment of acute SCI. While greater understanding of the optimal dosage, therapeutic time window and precise mechanism of action is needed, the present results are encouraging. The feasibility of conducting clinical trials of G-CSF treatment for acute SCI patients should be considered.

## Conclusions

G-CSF protects oligodendrocyte from SCI-induced cell death via the suppression of inflammatory cytokines and up-regulation of anti-apoptotic protein. As a result, G-CSF attenuates white matter loss and promotes hindlimb functional recovery.

## Materials and Methods

### Animals

All animals were treated and cared for in accordance with the Chiba University School of Medicine guidelines pertaining to the treatment of experimental animals. The present study was approved by Animal Care and Use committee of Chiba University Graduate School of Medicine (the approval number was 20060017). Ninety adult female Sprague-Dawley rats (10–12 weeks old; weight 200–240 g; Japan SLC, Inc. Hamamatsu, Japan) were housed in individual cages and given food and water *ad lib*. Rats were anesthetized with 1.5% halothane in 0.5 L/min oxygen and contused on T9 spinal cord exposed by a T8/9 laminectomy. Contusive SCI was introduced using the Infinite Horizon Impactor (Precision Systems and Instrumentation, Lexington, KY, magnitude: 200 kilo dyne). Upon awakening, rats were evaluated neurologically and were monitored for food and water uptake and urine output. As prophylactic, Bactramin (Chugai, Japan) was added to drinking water.

Rats were randomly assigned to two groups. G-CSF group received recombinant human G-CSF (15.0  $\mu$ g/kg; kindly provided by Kirin Pharma Co. Ltd., Tokyo, Japan), which was dissolved in normal saline. Vehicle group rats received equal volumes of normal saline at the same time points. All compounds were administered by tail vein injection at 1 h after surgery and daily the next four days. We followed the regimen of drug administration previously reported in the rat brain infarction model [13]. In addition, we performed preliminary experiments in other dose regimen (5, 15, 50  $\mu$ g/kg/d for 5 days after injury). Those preliminary data suggested that 15  $\mu$ g/kg/d G-CSF exerts most strong effects. Thus we employed 15  $\mu$ g/kg/d dose regimen. We collected peripheral blood 1 day after injury and counted



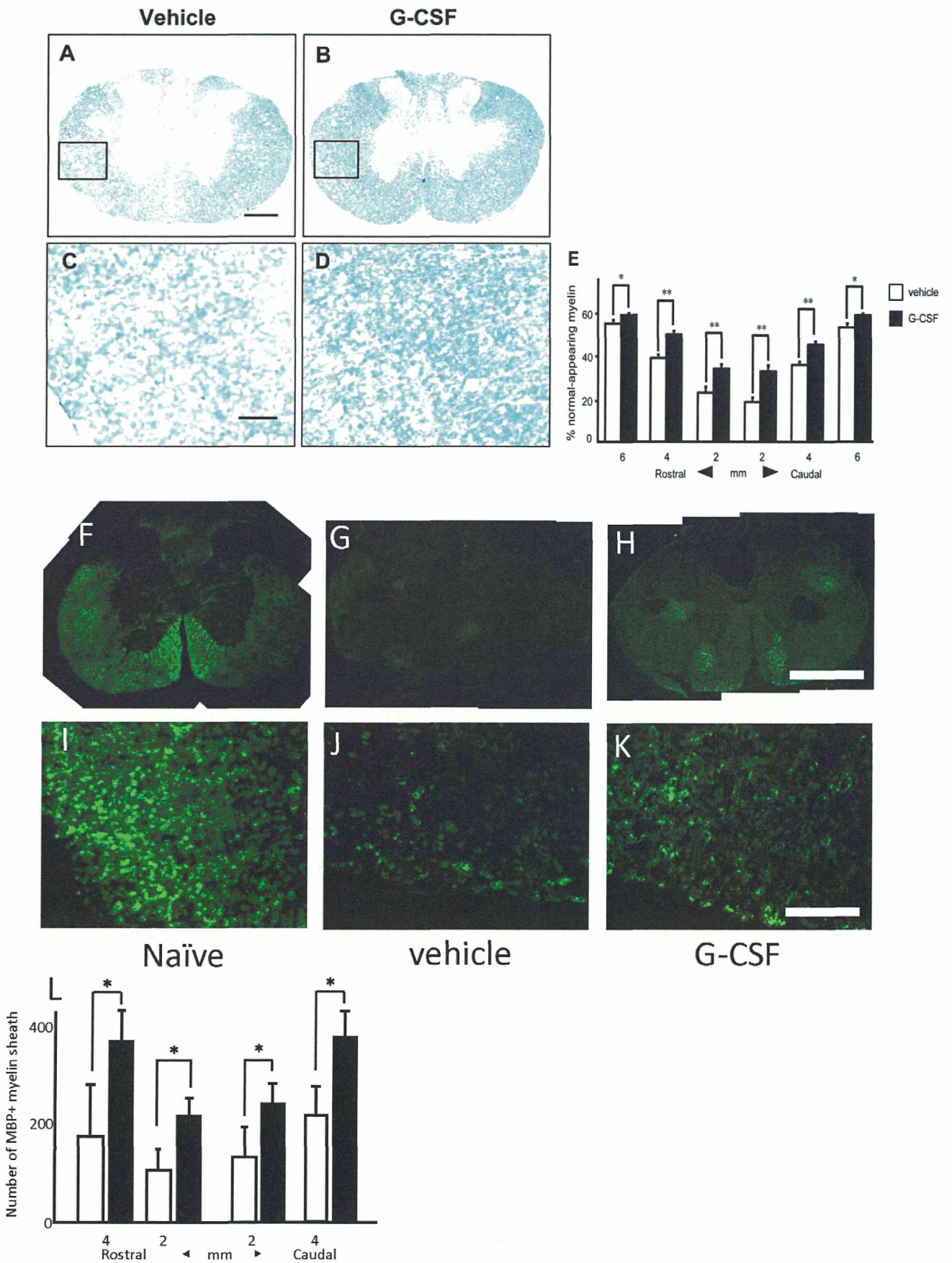


**Figure 5. G-CSF attenuated degeneration of white matter myelin.** Luxol Fast Blue (LFB) staining and immunofluorescent staining for myelin basic protein (MBP) were performed to quantify spared myelin in the chronic phase of SCI. Figures show LFB staining of the spinal cord 4 mm caudal to the epicenter. Higher magnification revealed better myelin integrity in rats from the G-CSF group (D) than the vehicle group (C). The extent of loss of myelin in the chronic phase of injury (six weeks after surgery) was analyzed (Fig. 4–E). Gray matter of each sample was subtracted from the whole area of the slice to reveal the area of white matter. The actual area of normal-appearing myelin was divided by the white matter to determine the percentage of normal-appearing myelin. The percentage of normal appearing myelin was significantly larger in the G-CSF group (E; closed column) than the vehicle group (E; open column). Immunofluorescence showed that the number of MBP-positive myelin sheath was larger in the G-CSF group than that in the vehicle group (L). Bars = 1 mm (F–H), 500  $\mu$ m (A, B) and 100  $\mu$ m (C, D, I–K), values are mean  $\pm$  SEM. \* $p$ <0.05, \*\* $p$ <0.01. Values are mean  $\pm$  SEM. \* $p$ <0.05, \*\* $p$ <0.01. Values are mean  $\pm$  SEM. \* $p$ <0.05, \*\* $p$ <0.01. doi:10.1371/journal.pone.0050391.g005

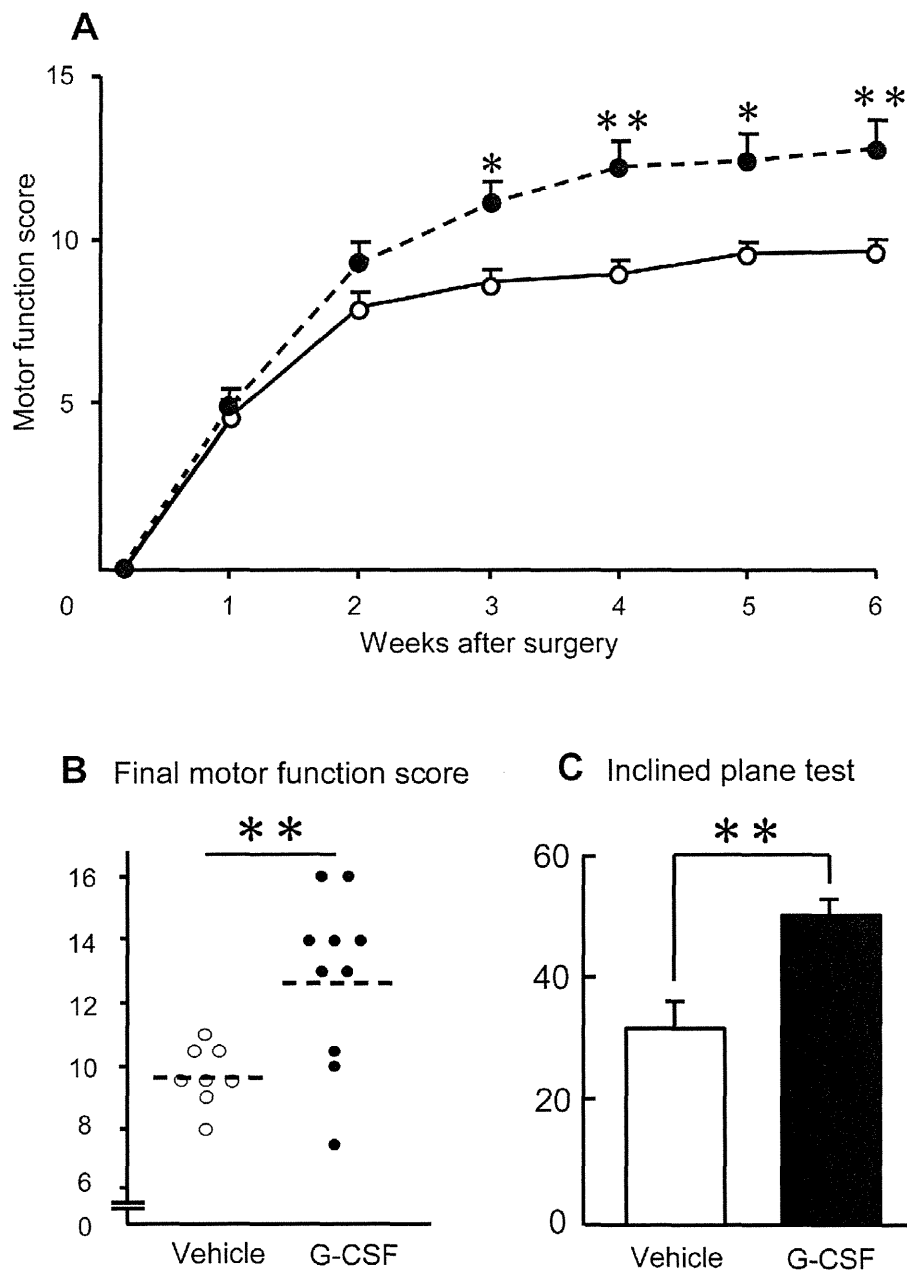


**Figure 6. Locomotor recovery.** Assessment of hind limb function with the Basso, Beattie and Bresnahan (BBB) locomotor scale (A, B). Time course of recovery of hindlimb function (A) and comparison of final motor function scores (B). Rats from the G-CSF group (closed circle) showed significant recovery compared to rats from the vehicle group (open circle) (A; Repeated measures ANOVA,  $p$ <0.05). The final motor function score six weeks after surgery in the G-CSF group (average 12.8; B, closed circle) was significantly higher than that in the vehicle group (average 9.7; B, open circle,  $p$ <0.01). The average score in the inclined plane test ten weeks after surgery in the G-CSF group (average 50 degrees; C, closed column) was significantly higher than that in the vehicle group (average 31.7 degrees; C, open column,  $p$ <0.01). Values are mean  $\pm$  S.E.M. \* $p$ <0.05, \*\* $p$ <0.01. doi:10.1371/journal.pone.0050391.g006



leukocyte number, the average of which was 3800 in the vehicle control group and 9700 in the G-CSF group.

### Real-Time Polymerase Chain Reaction (PCR) (Relative Quantitation)

We performed quantitative real-time PCR to determine expression of inflammatory cytokines. First-strand cDNA synthesis and Real-Time PCR were performed as previously described [11]. Briefly, for gene analysis, animals of each group were euthanized under pentobarbital anesthesia 12, 24 h and 72h after surgery ( $n = 5/\text{group}$ ) and 10 mm of spinal cord segment including lesion were removed, snap-frozen in liquid nitrogen, and stored at  $-80^{\circ}\text{C}$  until use. Total RNA was isolated from spinal cord samples using the RNeasy RNA isolation system (Qiagen Inc.) according to the manufacturer's instructions. Taqman technology (Model 7500 sequence detector, Applied Biosystems, Warrington, UK) was used for quantitative real-time PCR. All samples were run in duplicate. TaqMan probes (labeled with the fluorescent reporter FAM) for interleukin-1 beta (IL-1 $\beta$ ), tumor necrosis factor-alpha (TNF- $\alpha$ ), FAS, FAS ligand, interleukin-6, interferon-gamma (IFN- $\gamma$ ), matrix metalloproteinase-2 (MMP-2) and matrix metalloproteinase-9 (MMP-9) were designed by Applied Biosystems. Samples were tested in duplicate, and the average values of the threshold cycle (Ct) were used for quantification. To quantify the relative expression of each specific gene, the Ct values were normalized for endogenous 18S ribosomal RNA, and compared with a calibrator using the  $\Delta\Delta\text{Ct}$  method ( $\text{Ct} = \text{Ct}_{\text{Sample}} - \text{Ct}_{\text{Calibrator}}$ ) and converted to a logarithmic value. As calibrator, we used expression in the G-CSF group 12 h after surgery because the expression level of those cytokines in the normal spinal cord was very low. The mean result was further subjected to statistical analysis and expressed as fold-increase.

### Western Blot Analysis

Injured spinal cords (10-mm segments) were homogenized in a homogenization buffer (50 mM Tris-HCl (pH 7.4), 150 mM NaCl, 1% Triton X-100) containing a protease inhibitor cocktail (complete, Roche Diagnostics, Basel, Switzerland). Homogenates were cleared by centrifugation at 14,000 rpm for 10 min at  $4^{\circ}\text{C}$ . Protein concentration of supernatants was measured with Bio-Rad Dc Protein Assay Reagents (Bio-Rad Laboratories, Hercules, CA, USA), and the protein concentration was adjusted to 1 mg/mL by diluting supernatants with a homogenization buffer. Protein samples were mixed with an equal volume of a 2 $\times$ sample buffer (250 mM Tris-HCl, 4% sodium dodecyl sulfate (SDS), 20% glycerol, 0.02% bromophenol blue, and 10%  $\beta$ -mercaptoethanol). After boiling for 5 min, equal volumes of samples were subjected to 10% SDS-polyacrylamide gel electrophoresis (SDS-PAGE) under reducing conditions, and the proteins were transferred to a polyvinylidene difluoride membrane (Immobilon-P; Millipore Corporation, Billerica, MA, USA). After blocking of the membrane with PBS containing 5% skim milk and 0.05% Tween 20, the membrane was reacted with an anti-IL-1 $\beta$  (BD Biosciences, Franklin Lakes, NJ), an anti-TNF- $\alpha$  (BD Biosciences) and an anti- $\beta$ -actin antibody as a loading control (Santa Cruz Biotechnology, Santa Cruz, CA) antibody. For detection, a horse radish peroxidase-conjugated secondary antibody (Cell Signaling Technology, Beverly, MA, USA) and an ECL chemiluminescence system (GE Healthcare, Piscataway, NJ, USA) were used. Quantification of protein bands was performed using image J software.

### Tissue Preparation

For histological evaluation, animals were perfused transcardially with 4% paraformaldehyde in PBS (pH 7.4) under pentobarbital anesthesia 12, 24, 72 h and one week after surgery ( $n = 4/\text{group}$ ) and six weeks after surgery ( $n = 10/\text{group}$ ). Spinal cord tissue blocks including the lesion epicenter were removed and postfixed in the same fixative overnight, stored in 20% sucrose in PBS at  $4^{\circ}\text{C}$ , and embedded in OCT compound (Sakura Finetechnical, Tokyo, Japan). The cryoprotected samples were frozen and kept at  $-80^{\circ}\text{C}$  until use. The samples were cut into serial 10  $\mu\text{m}$  transverse sections with a cryostat and mounted on aminosilane-coated slides (Matsunami, Tokyo, Japan).

### Immunofluorescent Labeling

For immunofluorescent labeling, sections were permeated with 0.3% Triton X and treated for 1 h in blocking solution containing 1% bovine serum albumin and Block Ace (Dainippon Pharma, Japan). Sections were then incubated with the following primary antibodies as indicated: mouse monoclonal anti-G-CSF receptor antibody (G-CSFR, 1:200, Abcam, Cambridge, UK), rabbit polyclonal anti-microtubule associated protein-2 (MAP-2) antibody (MAP-2, 1:400, Chemicon Inc, Temecula, CA) for neurons, rabbit polyclonal anti-gial fibrillary acidic protein antibody (GFAP, 1:400, Sigma, St Louis, MO) for astrocytes, mouse monoclonal anti-adenomatous polyposis coli antibody (APC, 1:800, Calbiochem, San Diego, CA) or mouse monoclonal anti-myelin oligodendrocyte specific protein IgM antibody (MOSP, 1:200, Chemicon Inc) for oligodendrocytes, goat polyclonal anti-ionized calcium-binding adaptor molecule 1 (Iba-1, 1:500, Abcam) for microglia, rabbit polyclonal anti-activated caspase 3 antibody (Caspase 3-a, 1:400, R & D systems, Minneapolis, MN) for apoptotic cells, rabbit polyclonal anti-Bcl-XI antibody (1:200, AbD Serotec, Kidlington, UK), mouse monoclonal anti-IL-1 $\beta$  antibody (IL-1 $\beta$ , 1:200, AbD Serotec), rabbit polyclonal anti-myeloperoxidase antibody (MPO, prediluted, Abcam, Cambridge, UK) for infiltrating inflammatory leukocytes, mouse monoclonal anti-inducible nitric oxide synthase antibody (iNOS, 1:100, Chemicon Inc.), mouse monoclonal anti-arginase 1 antibody (1:100, Chemicon Inc.) and mouse anti-myelin basic protein antibody (MBP, 1:100, Chemicon Inc.) for myelin sheath. The sections were reacted with primary antibodies overnight at  $4^{\circ}\text{C}$ . After incubation with the primary antibodies, sections were washed in PBS and then incubated with secondary antibodies at room temperature for 1 h: Alexa 488- or 594- labeled anti-mouse, anti-rabbit IgG, anti-goat IgG or anti-mouse IgM antibodies (1:800, Molecular Probes, Eugene, OR). Finally, sections were washed twice in PBS and coverslips were added. The positive signals were observed by fluorescence microscopy (ECLIPSE E600; Nikon, Tokyo, Japan). In case of double staining for G-CSFR/GFAP and G-CSFR/MOSP, the positive signals were detected using confocal laser scanning microscopy (LSM5 PASCAL; Carl Zeiss, Germany). The specificity of the staining procedures was controlled by omitting primary or secondary antibodies.

On the sections from normal spinal cord and one week after surgery, immunofluorescence double labeling for G-CSFR and cell specific markers (MAP-2, GFAP, MOSP and Iba-1) was performed to elucidate the expression of G-CSFR. To detect the influence of G-CSF on G-CSFR expression in oligodendrocytes, quantification was performed by cell count of G-CSFR and MOSP-double positive cells one week after SCI.

To observe the effects of G-CSF on inflammatory cells, immunofluorescence for neutrophils and microglia were performed. Twelve and 24 h after surgery, IL-1 $\beta$ -expressing inflammatory leukocytes were counted as IL-1 $\beta$ - and MPO-double

positive cells. To quantitatively analyze the number of IL-1 $\beta$ - and MPO-double positive cells sections were picked from lesion epicenter and 2 mm rostral and caudal segments to the epicenter. Three samples from each segment were observed and a mean value of results was analyzed. The mean values of number of double-positive cells per section were compared between the groups. One week after the injury, phenotype of microglia/macrophage was determined by immunofluorescent double staining for Iba-1/iNOS or Iba-1/arginase-1. The number of total Iba-1-positive cells was counted, then the ratio between iNOS-positivity and arginase-positivity was calculated.

Apoptotic oligodendrocytes were counted as activated caspase 3 and APC-double positive cells in samples collected 72 h and one week after surgery. For the quantitative analysis of the number of apoptotic oligodendrocytes, sections were picked from epicenter, segments 2 mm, 4 mm and 6 mm rostral and caudal to the epicenter. The percentage of apoptotic oligodendrocyte was calculated by dividing the number of activated caspase 3 and APC-double positive cells by total APC-positive cell number. We also performed immunofluorescence double labelling for APC and one of the anti-apoptotic protein Bcl-Xl on spinal cord histological sections one week after injury.

To determine the influence of neuronal death on oligodendrocyte survival or death, we performed immunofluorescence for MAP-2 one week after the injury and counted the number of MAP-2-positive neurons in both the vehicle and G-CSF-treated rats.

For quantification of immunofluorescence data, every fifth ten- $\mu$ m transverse section (50  $\mu$ m apart) was picked from epicenter, 2 mm, 4 mm and 6 mm rostral or caudal to the lesion epicenter. At least ten sections per each animal were counted, resulting in coverage for 500  $\mu$ m area of spinal cord in each segment. To count positive cells, we used Scion Image computer analysis software (version beta 4.0.3, Scion Corporation, Frederick, MA).

### Myelin Sparing and Oligodendrocyte Cell Count

We performed luxol fast blue (LFB) staining and immunofluorescence for MBP to measure an area of spared white matter myelin six weeks after surgery. The LFB-positive area and total area of white matter of the same section was calculated using Scion Image computer analysis software. Gray matter was subtracted from the whole area of the slice to reveal the area of white matter. To determine the percentage of normal-appearing myelin, the area of the LFB stain was divided by the area of the white matter (Fig. 5 E). Immunofluorescent labeling for MBP was performed to quantify the number of MBP-positive myelin sheath six weeks after surgery as described above. The number of MBP-positive myelin sheath in white matter was counted (Fig. 5 F). Quantification was done as described above.

### Assessment of Locomotor Activity

The recovery of rat hindlimb function in both groups ( $n = 10$  in the G-CSF group and  $n = 8$  in the vehicle group) was determined by measuring the hindlimb motor function score with Basso, Beattie and Bresnahan locomotor scale (BBB scale [37]). Rats were allowed to move freely on the open field with a rough surface for five min at each time tested. The hindlimb movement of rats was scored by two independent observers who were unaware of the treatment. Measurement of motor function was performed weekly following the sixth week after surgery.

In another subset of rats treated the same as above, the inclined plane test was performed ten weeks after surgery as previously described [38] ( $n = 5$  in each group). The highest degree of

inclination was defined as that at which the animal could maintain its position for five seconds on two separate trials.

### Statistical Analysis

Results of immunohistochemical studies, percentages of normal-appearing myelin, final motor function scores and inclined plane tests were subjected to Student's t-test. Recovery of motor function scores was subjected to Repeated Measures ANOVA followed by post hoc test using Fisher's Protected Least Significant Difference test. Percentage of normal myelin (average values of sections) and final motor function scores were analyzed for the Pearson product-moment correlation coefficient. Results are presented as mean values  $\pm$  S.E. Values of  $p < 0.05$  were considered statistically significant.

### Supporting Information

**Figure S1 G-CSFR expression in naïve spinal cord. GFAP-positive astrocytes (A), MOSP-positive oligodendrocytes (B) and MAP-2-positive neurons (C) expressed G-CSFR.** Although the number of MOSP-positive oligodendrocytes was significantly different between the vehicle (D, open columns) and G-CSF groups (D, closed columns), all of the MOSP-positive oligodendrocytes expressed G-CSFR after SCI. Bar = 100  $\mu$ m. Values are mean  $\pm$  S.E.M. \* $p < 0.05$ . (TIF)

**Figure S2 The number of MAP-2-positive neurons after SCI.** The number of MAP-2-positive neurons was significantly larger in the G-CSF group in the rostral and caudal segments (closed columns). Values are mean  $\pm$  S.E.M. \* $p < 0.05$ . (TIF)

**Figure S3 The influence of G-CSF on microglia/macrophages.** Double immunofluorescence study for ionized calcium-binding adaptor molecule 1 (Iba-1, as a marker for activated microglia and macrophages) and inducible nitric oxide synthase (iNOS, as a marker for Th1-driven activation of microglia/macrophages) or arginase-1 (a marker for Th2-driven activation of microglia/macrophages) was performed to elucidate G-CSF-mediated reaction and phenotypic alteration of macrophage/microglia. The number of Iba-1-positive cells in the G-CSF group was significantly smaller than that in the vehicle group in the rostral and caudal segments, whereas the ratios between iNOS (open columns) and arginase-1 (hatched or dotted columns) did not change in both the vehicle and G-CSF groups in lesioned spinal cord at any segments observed. Values are mean  $\pm$  S.E.M. \* $p < 0.01$ . (TIF)

**Figure S4 Apoptotic oligodendrocytes.** To further confirm the results of immunohistochemistry for apoptotic oligodendrocytes, we performed double immunofluorescence study for MOSP as another marker for oligodendrocytes and activated caspase-3 as a marker for apoptotic cells (A-C). The staining pattern was similar to that of the double fluorescence study for APC and activated caspase-3. Co-localization of MOSP and activated caspase-3 was further confirmed with orthogonal imaging obtained by laser confocal microscopy (D). (TIF)

### Author Contributions

Conceived and designed the experiments: RK MK KT MY. Performed the experiments: RK MK JK MH YN CM TM TF AO. Analyzed the data: RK MK KT MY. Contributed reagents/materials/analysis tools: RK MK JK MH YN CM. Wrote the paper: RK MK MY.

## References

- Bauchet L, Lonjon N, Perrin FE, Gilbert C, Privat A, et al. (2009) Strategies for spinal cord repair after injury: a review of the literature and information. *Ann Phys Rehabil Med* 52: 230–251.
- Crowe MJ, Bresnahan JC, Shuman SL, Masters JN, Beattie MS (1997) Apoptosis and delayed degeneration after spinal cord injury in rats and monkeys. *Nat Med* 3: 73–76.
- Cao Q, Zhang YP, Iannotti C, DeVries WH, Xu XM, et al. (2005) Functional and electrophysiological changes after graded traumatic spinal cord injury in adult rat. *Exp Neurol* 191: S3.
- Fehlings MG, Tator CH (1995) The relationships among the severity of spinal cord injury, residual neurological function, axon counts, and counts of retrogradely labeled neurons after experimental spinal cord injury. *Exp Neurol* 132: 220–228.
- Park E, Velumian A, Fehlings MG (2004) The role of excitotoxicity in secondary mechanisms of spinal cord injury: a review with an emphasis on the implications for white matter degeneration. *J Neurotrauma* 21: 754–774.
- Bracken MB, Shepard MJ, Collins WF, Holford TR, Young W, et al. (1990) A randomized, controlled trial of methylprednisolone or naloxone in the treatment of acute spinal-cord injury. Results of the Second National Acute Spinal Cord Injury Study. *N Engl J Med* 17: 1405–1411.
- Hall ED, Springer JE (2004) Neuroprotection and acute spinal cord injury: a reappraisal. *Neuro Rx* 1: 80–100.
- Nicola NA, Metcalf D, Matsumoto M, Johnson GR (1983) Purification of a factor inducing differentiation in murine myelomonocytic leukemia cells: identification as granulocyte colony-stimulating factor. *J Biol Chem* 258: 9017–9023.
- Roberts AW (2005) G-CSF: a key regulator of neutrophil production, but that's no all! *Growth Factors* 23: 33–41.
- Jansen J Hanks S, Thompson JM, Dugan MJ, Akard LP (2005) Transplantation of hematopoietic stem cells from the peripheral blood. *J Cell Mol Med* 9: 37–50.
- Gibson CL, Bath PM, Murphy SP (2005) G-CSF reduces infarct volume and improves functional outcome after transient focal cerebral ischemia in mice. *J Cereb Blood Flow Metab* 25: 431–439.
- Komine-Kobayashi M, Zhang N, Liu M, Tanaka R, Hara H, et al. (2006) Neuroprotective effect of recombinant human granulocyte colony-stimulating factor in transient focal ischemia of mice. *J Cereb Blood Flow Metab* 26: 402–413.
- Schneider A, Krüger C, Steigleder T, Weber D, Pitzer C, et al. (2005) The hematopoietic factor G-CSF is a neuronal ligand that counteracts programmed cell death and drives neurogenesis. *J Clin Invest* 115: 2083–2098.
- Shābitz WR, Kollmar R, Schwanager M, Juettler E, Bardutzky J, et al. (2003) Neuroprotective effect of granulocyte colony-stimulating factor after focal cerebral ischemia. *Stroke* 34: 745–751.
- Six I, Gasan G, Mura E, Bordet R (2003) Beneficial effect of pharmacological mobilization of bone marrow in experimental cerebral ischemia. *Eur J Pharmacol* 458: 327–328.
- Shyu WC, Lin SZ, Lee CC, Liu DD, Li H (2006) Granulocyte colony-stimulating factor for acute ischemic stroke: a randomized controlled trial. *CMAJ* 174: 927–933.
- Kawabe J, Koda M, Hashimoto M, Fujiyoshi T, Furuya T, et al. (2011) Neuroprotective effects of granulocyte colony-stimulating factor and relationship to promotion of angiogenesis after spinal cord injury in rats. *J Neurosurg Spine* in press.
- Koda M, Nishio Y, Kamada T, Someya Y, Okawa A, et al. (2007) Granulocyte colony-stimulating factor (G-CSF) mobilizes bone marrow-derived cells into injured spinal cord and promotes functional recovery after compression-induced spinal cord injury in mice. *Brain Res* 1149: 223–231.
- Nishio Y, Koda M, Kamada T, Someya Y, Kadota R, et al. (2007) Granulocyte colony-stimulating factor (G-CSF) attenuates neuronal death and promotes functional recovery after spinal cord injury in mice. *J Neuropathol Exp Neurol* 66: 724–731.
- Osada T, Watanabe M, Hasuo A, Imai M, Suyama K (2010) Efficacy of the coadministration of granulocyte colony-stimulating factor and stem cell factor in the activation of intrinsic cells after spinal cord injury in mice. *J Neurosurg Spine* 13: 516–523.
- Pitzer C, Klussmann S, Krüger C, Letellier E, Plaas C, et al. (2010) The hematopoietic factor granulocyte-colony stimulating factor improves outcome in experimental spinal cord injury. *J Neurochem* 113: 930–942.
- Sanli AM, Serbes G, Calışkan M, Kaptanoğlu E, Sargon MF, et al. (2010) Effect of granulocyte-colony stimulating factor on spinal cord tissue after experimental contusion injury. *J Clin Neurosci* 17: 1548–1552.
- Loddick SA, Rothwell NJ (1996) Neuroprotective effects of human recombinant interleukin-1 receptor antagonist in focal ischemia in the rat. *J Cereb Blood Flow Metab* 16: 932–940.
- Zavala F, Abad S, Ezine S, Taupin V, Masson A, et al. (2002) G-CSF therapy of ongoing experimental allergic encephalomyelitis via chemokine- and cytokine-based immune deviation. *J Immunol* 168: 2011–2019.
- Boneberg EM, Hareng L, Gantner F, Wendel A, Hartung T (2000) Human monocytes express functional receptors for granulocyte colony-stimulating factor that mediate suppression of monokines and interferon  $\gamma$ . *Blood* 95: 270–276.
- Nishiki S, Hato F, Kamata N, Sakamoto E, Hasegawa T, et al. (2004) Selective activation of STAT 3 in human monocytes stimulated by G-CSF: implication in inhibition of LPS-induced TNF- $\alpha$  production. *Am J Physiol Cell Physiol* 286: 1302–1311.
- Squadrito F, Altavilla D, Squadrito G, Campo GM, Ioculano M, et al. (1997) The effects of recombinant human granulocyte-colony stimulating factor on vascular dysfunction and splanchnic ischaemia-reperfusion injury. *Br J Pharmacol* 120: 333–339.
- Lee S, Chu K, Jung K, Ko SY, Kim EH, et al. (2005) Granulocyte colony-stimulating factor enhances angiogenesis after focal cerebral ischemia. *Brain Res* 1058: 120–128.
- Takahashi JL, Giuliani F, Power C, Imai Y, Yong VW (2003) Interleukin-1beta promotes oligodendrocyte death through glutamate excitotoxicity. *Ann Neurol* 53: 588–595.
- Lee YB, Yune TY, Baik SY, Shin YH, Du S, et al. (2000) Role of tumor necrosis factor-alpha in neuronal and glial apoptosis after spinal cord injury. *Exp Neurol* 166: 190–195.
- Barres BA, Jacobson MD, Schmid R, Sendtner M, Raff MC (1993) Does oligodendrocyte survival depend on axons? *Current Biol* 3: 489–497.
- Blight AR (1983) Cellular morphology of chronic spinal cord injury in the cat: analysis of myelinated axons by line-sampling. *Neuroscience* 10: 521–543.
- Kwon BK, Tetzlaff W, Grauer JN, Beiner J, Vaccaro AR (2004) Pathophysiology and pharmacologic treatment of acute spinal cord injury. *Spine J* 4: 451–464.
- Jung K, Chu K, Lee ST, Kim SJ, Sinn DL, et al. (2006) Granulocyte colony-stimulating factor stimulates neurogenesis via vascular endothelial growth factor with STAT activation. *Brain Res* 1074: 190–201.
- Stroke Therapy Academic Industry Roundtable (STAIR) (1990) Recommendations for Standards Regarding Preclinical Neuroprotective and Restorative Drug Development. *Stroke* 30: 2752–2758.
- Schneider A, Wysocki R, Pitzer C, Krüger C, Laage R, et al. (2006) An extended window of opportunity for G-CSF treatment in cerebral ischemia. *BMC Biol* 4: 36.
- Basso DM, Beattie MS, Bresnahan JC (1995) A sensitive and reliable locomotor rating scale for open field testing in rats. *J Neurotrauma* 12: 1–21.
- Teng YD, Lavik EB, Qu X, Park KI, Ourednik J, et al. (2002) Functional recovery following traumatic spinal cord injury mediated by a unique polymer scaffold seeded with neural stem cells. *Proc Natl Acad Sci USA* 99: 3024–3029.

## CLINICAL CASE SERIES

# Anomalous Vertebral Arteries in the Extra- and Intraosseous Regions of the Craniovertebral Junction Visualized by 3-Dimensional Computed Tomographic Angiography

*Analysis of 100 Consecutive Surgical Cases and Review of the Literature*

Masashi Yamazaki, MD, PhD, Akihiko Okawa, MD, PhD, Takeo Furuya, MD, PhD, Tsuyoshi Sakuma, MD, Hiroshi Takahashi, MD, Kei Kato, MD, Takayuki Fujiyoshi, MD, PhD, Chikato Mannoji, MD, PhD, Kazuhisa Takahashi, MD, PhD, and Masao Koda, MD, PhD

**Study Design.** Consecutive case series and literature review.

**Objective.** To describe the utility of 3-dimensional computed tomographic angiography (3D CTA) for evaluating vertebral artery (VA) anomalies before surgery.

**Summary of Background Data.** Recent advances in instrumentation surgery at the craniovertebral junction (CVJ) enable us to perform rigid internal fixation. However, the risk of VA injury as a complication of the surgery has become a major problem. Thus, the importance of preoperative evaluation of the VA course has been emphasized.

**Methods.** Cases of 100 consecutive patients who underwent CVJ instrumentation surgery since July 1998 were analyzed. Occipitocervical/thoracic or C1–C2 posterior fusion was performed for atlantoaxial subluxation (AAS) in 59 patients and cervical fixation including C2 was required for middle-to-lower cervical lesions in 41 patients. Twenty-seven patients with AAS had a congenital skeletal anomaly (CSA) at the CVJ including os odontoideum and occipitalization of C1 (AAS-CSA[+] group). Anomalous VAs at the extra- and intraosseous regions were evaluated by 3D CTA.

**Results.** No neurovascular injury occurred during surgery. Abnormal courses of the VA at the extraosseous region were detected in 10 cases: 2 had fenestration and 8 had a persistent first intersegmental

artery. All 10 cases were in the AAS-CSA(+) group. A high-riding VA was detected in 31 cases. Fourteen out of the 31 cases were in the AAS-CSA(+) group, indicating 51.9% of the AAS-CSA(+) group had high-riding VA. In the AAS-CSA(+) group, a C1–C2 transarticular screw and C2 pedicle screw were actually inserted in 58% and 31% of the planned insertions, respectively.

**Conclusion.** The present findings suggest that the frequency of an abnormal VA at the extra- and intraosseous regions is increased when patients have AAS and CSA at the CVJ. Using preoperative 3D CTA, we can precisely identify anomalous VAs and thereby reduce the risk of their intraoperative injury.

**Key words:** vertebral artery, 3-dimensional computed tomography angiography, anomaly, craniovertebral junction. **Spine 2012; 37:E1389–E1397**

Recent advances in instrumentation surgery at the craniovertebral junction (CVJ) enable us to perform rigid internal fixation.<sup>1</sup> However, the risk of injury to the vertebral artery (VA) as a complication of surgery has become a major problem. A large-scale investigation of 1318 patients who underwent surgery for C1–C2 transarticular screw (TAS) fixation showed that VA injury occurred in 4.1% of patients and some of them developed cerebellar infarction or brain stem infarction.<sup>2</sup> Thus, the importance of preoperative evaluation of the VA course has been emphasized.

Previous studies have shown anomalies of the VA at the extra- and intraosseous regions of the CVJ.<sup>3–9</sup> There are 2 representative anomalies of the extraosseous course of the VA: fenestration and persistent first intersegmental artery (Figure 1A, B). In the former, the VA is duplicated after emerging from the C2 transverse foramen; one branch enters the spinal canal between C1 and C2 and the other courses normally, passing through the C1 transverse foramen and entering the spinal canal at the cranial side of the C1 posterior arch (Figure 1A).<sup>3,4</sup> In the latter, the VA enters the spinal canal at

From the Department of Orthopaedic Surgery, The Spine Section, Chiba University Graduate School of Medicine, Inohana, Chuo-ku, Chiba, Japan.

Acknowledgment date: November 30, 2011. First revision date: June 10, 2012. Acceptance date: July 16, 2012.

The device(s)/drug(s) is/are FDA-approved or approved by corresponding national agency for this indication.

Institutional funds were received to support this work.

No benefits in any form have been or will be received from a commercial party related directly or indirectly to the subject of this manuscript.

Address correspondence and reprint requests to Masashi Yamazaki, MD, PhD, Department of Orthopaedic Surgery, Spine Section, Chiba University Graduate School of Medicine 1-8-1, Inohana, Chuo-ku, Chiba 260-8670, Japan; E-mail: masashiy@faculty.chiba-u.jp

DOI: 10.1097/BRS.0b013e31826a0c9f

Spine

www.spinejournal.com E1389

Copyright © 2012 Lippincott Williams & Wilkins. Unauthorized reproduction of this article is prohibited.

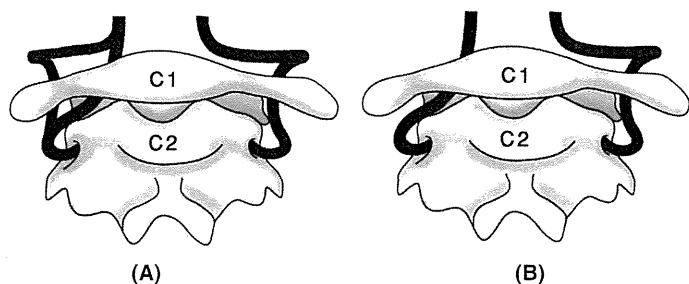


**Figure 1.** Two representative VA anomalies at the CVJ. (A) Fenestration. (B) Persistent first intersegmental artery. VA indicates vertebral artery; CVJ, craniovertebral junction

the caudal portion of the C1 posterior arch after emerging from the C2 transverse foramen, without passing through the C1 transverse foramen (Figure 1B).<sup>5,6</sup> Studies have also demonstrated a side-to-side asymmetry of bilateral VAs. In some patients, the lumen diameter of the VA on one side was more than twice that of the other side.<sup>5</sup> When an intraosseous VA is anomalously located too medially, too posteriorly, and/or too high, it is described as “high-riding.”<sup>5</sup>

We have performed 3-dimensional computed tomographic angiography (3D CTA) to analyze the extra- and intraosseous course of the VA before instrumentation surgery at the CVJ to avoid intraoperative VA injury.<sup>3-6</sup> In the present study, we investigated the presence of congenital skeletal anomaly (CSA) at the CVJ in 100 consecutive patients who underwent instrumentation surgery at the CVJ and analyzed the association of CSA with extra- and intraosseous anomalies of the VA.

**MATERIALS AND METHODS**

We analyzed 100 consecutive patients who underwent instrumentation surgery at the occiput, C1, and C2 at our institute between July 1998 and January 2009 (Table 1). Fifty-nine patients had atlantoaxial subluxation (AAS; AAS group), and cervical fixation including C2 was required for a middle-to-lower cervical spine lesion (MLCSL) in 41 patients (MLCSL group). The AAS group included 22 patients with cervical myelopathy because of CSA, such as os odontoideum, bifid C1 posterior arch, and occipitalization of C1. This group also included 12 patients with rheumatoid arthritis, 8 with dens fracture, 6 with AAS of unknown origin, 5 with Down syndrome, 3 with cerebral palsy, and 3 with trauma. All of the 5 patients with Down syndrome also had CSA including os odontoideum and bifid C1 posterior arch. Among the 59 patients in the AAS group, 27 patients had CSA at the CVJ (AAS-CSA[+] group) and the other 32 had no osseous anomaly (AAS-CSA[-] group) (Table 1). Details of the type of anomaly are shown in Table 2. The MLCSL group included 11 patients with a spine tumor, 10 with cervical spondylosis, 8 with cerebral palsy, 7 with ossification of the posterior longitudinal ligament (OPLL), 2 with a spinal cord tumor, 1 with CSA, 1 with neurofibromatosis, and 1 with trauma. Among the 41 patients in the MLCSL group, only 1 patient had CSA at the CVJ (MLCSL-CSA[+] group) and the other 40 had no osseous anomaly (MLCSL-CSA[-] group) (Tables 1 and 2).

**TABLE 1. Clinical Data for the 100 Study Cases**

	AAS Group	MLCSL Group
Total cases	59	41
Sex		
Male	25	29
Female	34	12
Congenital skeletal anomaly		
CSA(-)	32	40
CSA(+)	27*	1
Method of surgery		
Occ-C/T	36	2
C1-C2	23	0
C2-C/T	0	39

\*P < 0.01 vs. MLCSL group.  
 AAS indicates atlantoaxial subluxation; MLCSL, middle-to-lower cervical spine lesion; CSA, congenital skeletal anomaly; Occ-C/T, occipitocervical or occipitothoracic posterior fusion; C1-C2, atlantoaxial posterior fusion; C2-C/T, midcervical or cervicothoracic posterior fusion including axis.

The surgical methods in the AAS group were occipitocervical or occipitothoracic (Occ-C/T) posterior fusion (36 patients) and atlantoaxial (C1-C2) posterior fusion (23 patients). Patients in the MLCSL group underwent Occ-C/T posterior fusion surgery (2 patients) and midcervical or cervicothoracic posterior fusion including C2 (39 patients).

In patients who underwent Occ-C/T or C1-C2 posterior fusion, we used C1-C2 TAS as anchors to C2 from July 1998 through October 2005, and a C2 pedicle screw (PS) from November 2005. In patients who underwent midcervical or cervicothoracic posterior fusion including C2, we used C2 PS as anchors to C2 throughout the entire period.

**TABLE 2. Types of Congenital Skeletal Anomaly**

	AAS Group (n = 27)	MLCSL Group (n = 1)
Os odontoideum	18	
Os odontoideum, Bifid C1 posterior arch	2	
Os odontoideum, C1 occipitalization	1	
Os odontoideum, Klippel-Feil	1	
C1 occipitalization, Klippel-Feil	1	1
Hypoplastic odontoid/C1 posterior arch, SED	1	
Hypoplastic odontoid, SED	1	
Hypoplastic C1 posterior arch, SED	1	
Hypoplastic C1 posterior arch, DD	1	

AAS indicates atlantoaxial subluxation; MLCSL, middle-to-lower cervical spine lesion; SED, spondyloepiphyseal dysplasia; DD, diastrophic dysplasia.